ORIGINAL PAPER

D. Upadhyay · M. M. Raith · K. Mezger
A. Bhattacharya · P. D. Kinny

Mesoproterozoic rifting and Pan-African continental collision in SE India: evidence from the Khariar alkaline complex

Abstract The suture zone between the Bhandara craton and the granulite-facies rocks of the Eastern Ghats Province in SE India contains a number of deformed alkaline and tholeiitic intrusives. The Khariar alkaline complex is one of the several occurrences which intruded in the Mesoproterozoic (1,480 ± 17 Ma, 2σ) and was deformed during the Pan-African tectonothermal event. The geochemical signatures indicate a rift-related setting for the magmatic activity. The nepheline syenite parent magma may have been produced by in-mantle fractionation of clinopyroxene and Ti-rich amphibole from a basanitic primary magma derived from an enriched spinel lherzolite mantle source in the sub-continental lithosphere. Geochemical variations in the Khariar alkaline suite can be modeled by the fractionation of clinopyroxene, amphibole, titanite, zircon, apatite and allanite. The Mesoproterozoic alkaline magmatism at Khariar marks the initiation of a NE-SW rift which formed several craton margin basins and opened an ocean towards the south. The sediments of the cratogenic basins and the Eastern Ghats Province were deposited in these rift-related basins. A K-Ar age of 1,330 ± 53 Ma from glauconites in sandstone suggests
that the NW-SE trending Godavari–Pranhita graben formed at approximately the same time as the rift at the craton margin. If the two are related, the Godavari–Pranhita graben may represent the failed arm of a rift system in which the NE-SW arm was the active segment. The granulite-facies deformation and metamorphism of the Eastern Ghats Province sediments may be related to an episode of Grenvillian basin inversion. The Mesoproterozoic rifting and Grenvillian basin closure may thus represent two well-defined parts of a Wilson cycle i.e. the opening and closure of an ocean. The Khariar and other alkaline bodies were, however, deformed during a Pan-African collisional event associated with the westward thrusting of the Eastern Ghats Province granulites over the cratonic foreland.

D. Upadhyay · M. M. Raith
Mineralogisch-Petrologisches Institut, Poppelsdorfer Schloss,
Universität Bonn, 53115 Bonn, Germany

K. Mezger · *Present address*: D. Upadhyay (✉)
Zentrallabor für Geochronologie, Institut für Mineralogie,
Universität Münster, Corrensstrasse 24, 48149 Münster, Germany
E-mail: dewa_u@yahoo.co.in
Tel.: +49-251-8336107
Fax: +49-251-8338397

A. Bhattacharya
Department of Geology and Geophysics,
Indian Institute of Technology, 721302 Kharagpur, India

P. D. Kinny
Tectonics Special Research Centre, Department of Applied
Geology, Curtin University of Technology,
6845 Perth, Western Australia

Introduction

In Precambrian terranes, the identification of paleo-rifts is often complicated due to the modifying effects of subsequent deformation and metamorphism. Such rifts however, can be delineated along old continental sutures (Burke et al. 2003) where the emplacement of nepheline syenite complexes have been considered to be important markers of rift-related activity (Platt 1996).

In south eastern India, the suture zone between the Bhandara/Eastern Dharwar cratons (EDC) and the Eastern Ghats Belt (EGB) contains numerous deformed alkaline intrusives of Proterozoic age (Fig. 1, inset). The occurrence of alkaline complexes at this junction where crustal segments of contrasting affinities are juxtaposed against each other (i.e. dominantly Archaean cratonic rocks to the west and Proterozoic granulites to the east) has important implications for understanding the Proterozoic tectonics and juxtaposition of Peninsular India.

This contribution presents the results of a detailed geochemical and geochronological study of the Khariar alkaline complex and its neighboring crustal domains at the SE margin of the Bhandara craton (Fig. 1).

Fig. 1 Geological map of the Khariar nepheline syenite complex and adjacent crustal domains (modified after Madhavan and Khurram 1989) showing the locations of studied samples (the prefix DU to the sample numbers is omitted for clarity). The region enclosed by the *dotted rectangle* between 20°15 and 20°20N was mapped in detail in this study to bring out the relationship between the different units. The *inset* shows the Eastern Ghats Belt in peninsular India (modified after Dobmeier and Raith 2003) with the locations of the Khariar alkaline complex and the other important alkaline bodies along the suture with the Bhandara and Eastern Dharwar cratons
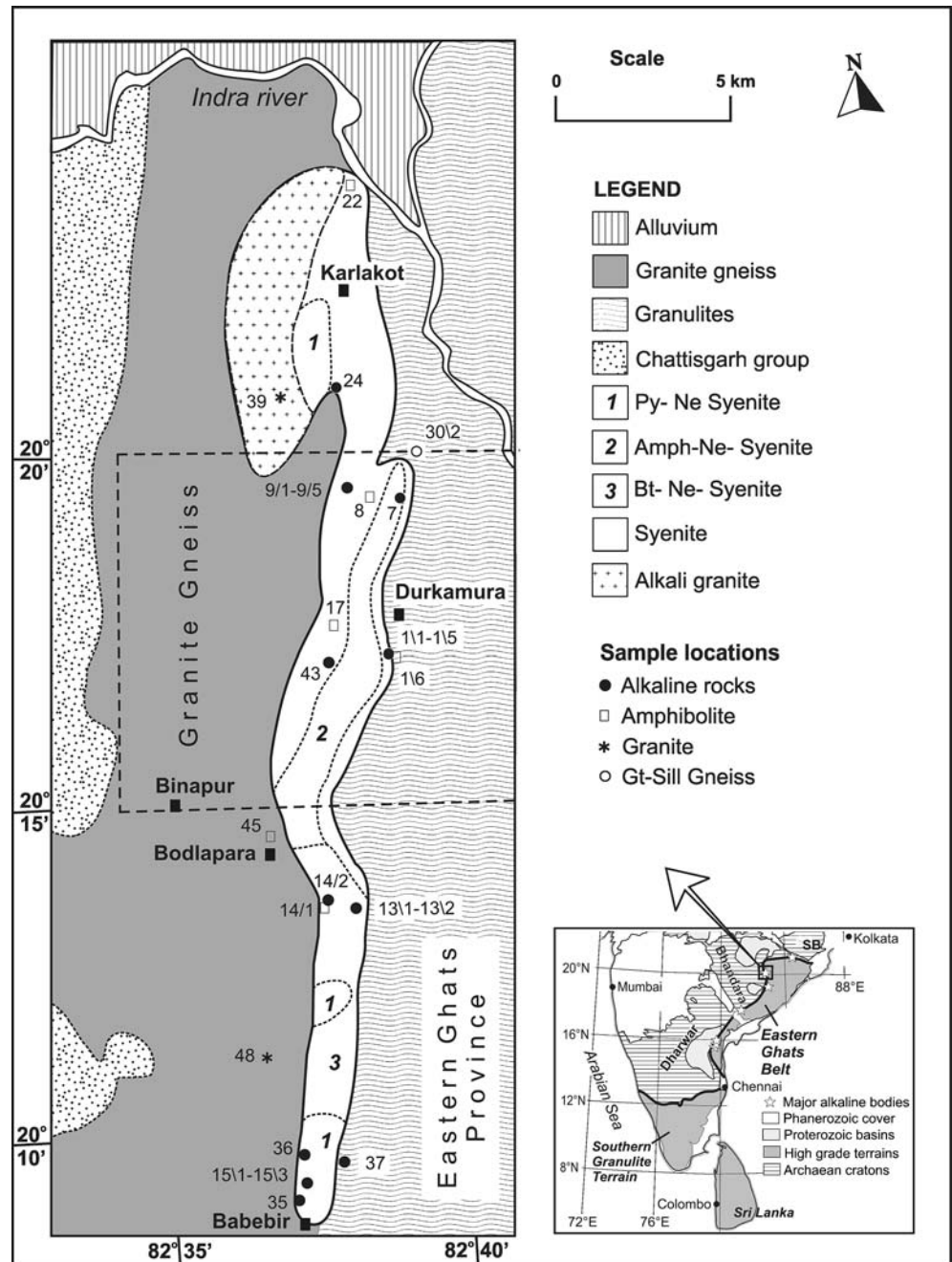
Integrating the results of the study with published geochronological and tectonic constraints from the region, permits one to formulate a coherent model for the evolution of the craton-EGB contact, which, attempts to integrate the geological evolution of the region by offering new prospects for the formation and disintegration of any pre-Rodinian supercontinent assembly.

Regional geology and field relations

The Khariar alkaline complex is similar to a number of other Si-undersaturated alkaline intrusives within the craton–EGB contact zone. The complex is sandwiched between granulite-facies rocks of the EGP (Dobmeier and Raith 2003) of the EGB to the east, and basement granites of the Bhandara craton to the west (Figs. 1, 2).

The Bhandara craton is a poorly studied entity in terms of its lithological components, tectonic divisions and geodynamic evolution. Its southern part is dominated by granitoids which include older gneissic enclaves of deformed tonalite-trondhjemite-granodiorite (TTG), supracrustals and late K-feldspar rich leucocratic granites (cf. Sarkar et al. 1993). Sarkar et al. (1993) reported upper intercept zircon ages of $3,509 + 14/-7$ and $2,480 \pm 3$ Ma for the Markampara trondhjemite gneiss
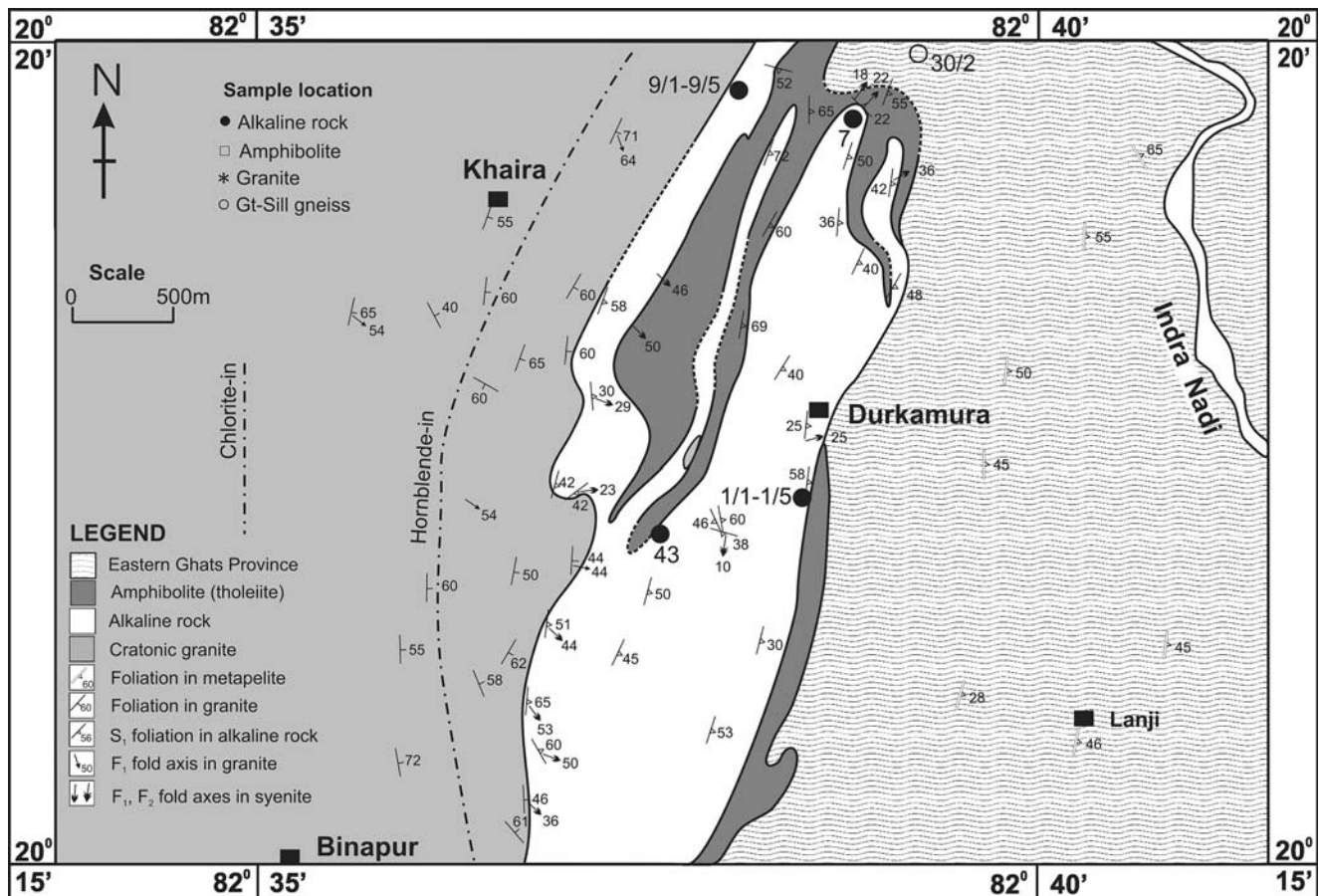
Fig. 2 Geological map of an east-west transect (as marked in Fig. 1) across the craton-EGB boundary showing the relationship between the tholeiites-alkaline rocks and the basement granites. The *dot-dash lines* in the granites mark the chlorite-in and the hornblende-in isograd documenting the decrease in metamorphic grade from the contact with the nepheline syenites into the hinterland. Note the 'xenolithic' band of granite within the nepheline syenite and the folded nature of the contact between the lithologies

and late granite respectively, which indicate Archean to early Paleoproterozoic crust formation in the cratonic foreland. The cratonic basement west of the Khariar alkaline complex is represented by granites and granite gneisses that show a westward decrease in the intensity of deformation and metamorphism resulting in mappable 'hornblende-in' and 'chlorite-in' isograds (Fig. 2). The ferromagnesian minerals defining the monophase fabric in the granites vary from amphibole–biotite–clinozoisite near to the contact with the alkaline rocks grading into chlorite–clinozoisite–biotite assemblage in the foreland zones. The granites adjacent to the syenites are essentially an amphibolite-facies L–S tectonite with the L-fabric defined by stretched K-feldspar grains. With increasing distance from the syenites, the S-fabric weakens as the metamorphic intensity decreases (Fig. 2) grading to almost undeformed granites in the foreland. S–C fabric in the granites indicates top-to-the-west thrusting. An alkali-granite body, mineralogically and chemically different from the foliated basement granite gneiss, forms a distinct occurrence at the northwestern margin of the alkaline complex (Fig. 1).

Although the timing of granitoid magmatism in this part of the craton is not known, a Paleoproterozoic ($\approx$2.6 Ga) depleted mantle (DM) Nd model age for the granite sample DU-48 (Table 4) indicates that the basement may have stabilized as early as 2.5 Ga. The basement is overlain by intra-cratonic sediments of the Chattisgarh Basin which are interpreted to have been deposited in an extensional regime along a passive Atlantic-type craton margin (Kale 1991, 1995). The sediments are estimated to have been deposited between 1,600 and 700 Ma (Kale 1991) but precise age determinations are not available.

The EGB, juxtaposed against the alkaline complex, is considered to be a Proterozoic orogen associated with Indo-Antarctic collisional events (Grew and Manton 1986; Mezger and Cosca 1999; Dasgupta and Sengupta 2003; Dobmeier and Raith 2003). The belt is a poly-deformed and poly-metamorphosed terrane comprising of granulite-facies paragneisses which host intrusives of charnockites, enderbites, massif-type anorthosites, megacrystic granitoids and alkaline rocks. On the basis of recent isotopic data, Dobmeier and Raith (2003) have

subdivided it into a number of 'provinces' having contrasting evolutionary histories. The high-grade EGB gneisses bordering the alkaline complex form a part of the EGP and include garnetiferous migmatized mafic granulites, garnet-corundum-sillimanite-bearing metapelites, quartzites, calc-silicate granulites and migmatized garnetiferous quartzo-feldspathic gneisses. The dominantly metapelitic rocks have undergone at least one granulite-facies migmatisation and deformation event in which garnet and orthopyroxene-bearing leucosomes formed. At the western margin, an amphibolite-facies mylonitic shear fabric is seen to overprint the earlier high-grade fabric of the EGP rocks. Biswal and Jena (1999) attributed the formation of this zone to retrogression of the granulites to amphibolites and schists due to the greenschist-amphibolite-facies P–T conditions during the westward thrusting of the EGP over the craton.

The Khariar alkaline complex occurs as a ~30 km long NE-SW trending sinuous belt and includes a differentiated magmatic suite dominated by nepheline syenites in the core and syenites along the marginal zones. The different petrographic varieties are not exclusive to either of these two zones because inter-layered and gradational relations among them are also observed. More mafic members of the suite include subordinate occurrences of thick to thin layers or lenses of mesocratic nepheline syenite and ijolite within the nepheline syenite. The rocks of the alkaline suite are at places intricately inter-layered with tholeiites occurring as persistent and traceable units of amphibolites both within the alkaline rocks and at the periphery of the complex (Fig. 2). The tholeiites may be the remnants of a tectonically-emplaced ocean floor. The rocks of the complex are strongly deformed and metamorphosed with the development of a gneissic foliation that overprints igneous layering. The earliest folds (F_1) affecting magmatic layering (S_0) are isoclinal, with the development of a penetrative axial planar foliation (S_1) defined by amphibole and biotite replacing clinopyroxene. The S_0–S_1 composite is refolded by a set of open to tight westerly overturned asymmetric folds (F_2). In zones of high F_2 strain near the eastern margin of the complex, a shear fabric (S_2) draws into parallelism all earlier structures. C–S fabric and other shear sense indicators suggest a northwest vergent movement on the shear fabric.

Petrography

In the nepheline syenites and the syenites, the feldspars are perthites and show varying degrees of microclinisation with extensive albite exsolution. Nepheline occurs both as coarse subhedral crystals and as smaller grains interstitial to the feldspars. Aligned grains of amphibole and biotite replacing clinopyroxene, and pinned aggregates of recrystallised feldspar define the S_1 fabric in these rocks. The accessory phases include calcite,

allanite, titanite, apatite, zircon, oxides and sulfides (pyrite, ilmenite, chalcopyrite, pyrrhotite and magnetite with ilmenite exsolution). Coronitic and skeletal garnets replace clinopyroxene, amphibole, plagioclase and calcite in some varieties. Nepheline shows replacement by cancrinite especially at contacts with carbonate. The mesocratic nepheline syenites and ijolites are comparatively mildly deformed coarse-grained rocks, with a weak planar anisotropy defined by amphibole in a partially recrystallised mosaic of clinopyroxene, nepheline and feldspars. Minor phases include calcite and titanite. Some clinopyroxenes in the ijolite occur as large megacrystic grains and may be of cumulus origin.

The tholeiites are dominated by clinopyroxene and plagioclase, with titanite and apatite as accessory phases. Brown amphibole replaces clinopyroxene and plagioclase and defines both the S_1 and the S_2 fabrics. Garnets are rare, but always skeletal, and overgrow the fabrics. Some tholeiites show evidence of fenitization by a silica-undersaturated alkaline fluid. The metasomatic textures include micro-veining and symplectitic replacement of plagioclase by nepheline.

The cratonic granites are dominated by quartz and alkalifeldspar > > plagioclase, amphibole, biotite, clinozoisite and chlorite. The accessory phases include titanite, zircon and minor ilmenite. The alkali granites, in contrast, contain dark green alkali clinopyroxene, bluish-green amphibole and biotite with some varieties rich in opaque phases.

Geochemistry

Analytical techniques

The whole-rock major element concentrations were measured at the Mineralogisch-Petrologisches Institut, University of Bonn, by X-ray fluorescence spectrometry on fused discs with a Philips PW-1480 X-ray spectrometer. The abundances of the REE, Y and Sc in some samples were determined using ICP-AES (VARIAN, Vista MPX axial) at Geoforschungszentrum (GFZ), Potsdam. Details of the analytical technique are given in Zuleger and Erzinger (1988). The other trace elements were analyzed by ICP-MS (VG-Plasma Quad PQ 2+) at GFZ, Potsdam. The external reproducibility of the concentrations is better than 10% for most elements as seen from the analyses of JB-3 reference basalt (Govindaraju 1994) (Table 3).

Whole-rock Sm-Nd and Rb-Sr isotopic ratios were measured on a Finnigan MAT multicollector thermal ionization mass spectrometer at the Institut für Geologische Wissenschaften, Freie Universität, Berlin. Repeated analysis of NBS 987 Sr and La Jolla Nd standard yielded mean values of 0.710351 ± 92 (2σ, 17 analyses) and 0.511817 ± 26 (2σ, 12 analyses) for the $^{87}Sr/^{86}Sr$ and $^{143}Nd/^{144}Nd$ ratios respectively. The isotopic ratios of the samples were corrected to account for the recommended values of 0.71024 and 0.511858 of the

NBS 987 Sr and La Jolla Nd standards (Lugmair et al. 1983). Pb isotopic ratios from leached feldspar separates and Rb–Sr isotopic ratios in biotites were measured at the Zentrallaboratorium für Geochronologie, University of Münster, on a VG sector 54 mass spectrometer fitted with nine faraday cups. Seven analyses of the NBS 982 Pb standard gives mean values of $0.027289 \pm 0.10\%$ (2σ), $0.466665 \pm 0.057\%$ (2σ) and $0.998623 \pm 0.11\%$ (2σ) for the $^{204}Pb/^{206}Pb$, $^{207}Pb/^{206}Pb$ and $^{208}Pb/^{206}Pb$ ratios respectively. The measured isotopic ratios of the feldspars were corrected for mass discrimination by a factor of 0.08% per amu.

Zircons were analyzed using the SHRIMP II ion microprobe at the John de Laeter Centre for Mass Spectrometry, Perth, Western Australia. Details of the analytical technique can be found in Compston et al. (1984). Cathodoluminescence (CL) imaging was conducted on a Philips XL30 Scanning Electron Microscope to reveal internal structures and as a guide to analytical spot selection. SHRIMP dating was done under routine operating conditions of 4nA O^{2-} primary beam current, 25 μm analytical spot, six-scan duty cycle and mass resolution 5,000+. Analyses of zircon standard CZ3 (564 Ma; $^{206}Pb/^{238}U = 0.0914$; 551 ppm U) were interspersed with analyses of the samples. The compiled data for the standard was used to correct the measured Pb/U ratios for instrumental discrimination and calibration of elemental concentrations. Common Pb correction was less than 1.2% of the ^{206}Pb counts for the high-U interior parts of the grains and was based on the measured ^{204}Pb. It was, however, significantly higher (up to 16.7%) for the analyses of the low-U outer parts of the grains.

In situ dating of monazites from a garnet-sillimanite gneiss belonging to the EGP was done at the Mineralogisch-Petrologisches Institut, University of Bonn, using a WDS Cameca Camebax Microbeam electron probe operating at an accelerating voltage of 20 kV and a beam current of 50 nA. The intensities of the U (M_β), Th (M_α), Pb (M_α) and Y (L_α) peaks were determined with counting times of 100 s for the peak and 50 s on the background for U, Th and Pb and 40 and 20 s for Y, respectively. UO_2, ThO_2, a pyromorphite ($Pb_5[Cl(PO_4)_3]$) and synthetic YPO_4 (Smithsonian Institution, see Jarosewich and Boatner 1991) were used as standards. Matrix correction was done using the PAP program of Pouchou and Pichoir (1984). Calculation of individual ages and age populations followed the procedure described in Montel et al. (1996).

Geochronological relationships

The results of the SHRIMP analyses on zircons from a nepheline syenite sample are listed in Table 1. A total of 10 grains representing 21 spots were analyzed. In most grains, the CL images reveal a poorly luminescent interior partly or totally enveloped by a more brightly luminescent exterior (Fig. 3b, c). The interiors show either a weak concentric zonation, or sector zoning, or irregular patchy zonation. The luminescent exteriors can be grouped into two types. In some crystals, the exteriors show weak concentric zones which follow the crystal faces of the interior regions; in others, the exterior truncates the internal zonation along irregular boundaries, while some grains show both features. The internal structure can be explained by a three stage evolution of the zircon grains. The interiors probably crystallized during the early stages of melt evolution and thus have high concentrations of U-Th (average U concentrations $\sim$150 ppm; and Th/U ratio >1; Table 1), while the concentrically zoned exteriors represent overgrowths formed during the later stages of melt differentiation. They have much lower concentrations of U–Th (average U concentrations $\sim$20 ppm; and Th/U ratio of 0.2–0.3; Table 1) because the melt must have been depleted in these components by then. This interpretation is supported by the differentiation scheme (discussed below) that requires the fractionation of accessory phases like allanite, titanite, apatite and zircon, which would deplete the melts in U–Th. Moreover, the concentrically zoned outer regions yield overlapping ages, albeit with large uncertainty, as the interiors which further imply that the two may have been coeval. The luminescent exteriors of some grains however, give the impression that they have encroached upon and replaced the zoned exteriors and the interiors by recrystallisation. The irregular shapes and uneven development of these brighter outer zones suggests that the implied recrystallization could have been driven by fluid interaction. These irregular zones may have overgrown the interior and the zoned exteriors during the metamorphic overprint on the rocks.

The 11 spots that represent the more precise analyses of the interiors give a mean $^{207}Pb/^{206}Pb$ age of $1,488 \pm 24$ Ma (95% confidence), but the data show a slight scatter about the mean (chi-square value 1.86). Omitting analysis 10b as an outlier gives a mean age of $1,480 \pm 17$ Ma (2σ) which is interpreted to date magmatic crystallization and hence the emplacement of the Khariar alkaline rocks (Fig. 3a). The $^{207}Pb/^{206}Pb$ age is similar to the $1,500 + 3/-4$ Ma U-Pb TIMS upper intercept age obtained by Aftalion et al. (2000) for zircon crystals from a syenite pegmatite belonging to the same suite.

Aftalion et al. (2000) also reported a zircon lower intercept age of 540 ± 20 Ma which may date the subsequent metamorphic overprint on the alkaline rocks and account for the recrystallized outer zones of the zircons and the discordance in the analyses. This Pan-African age of the tectonothermal overprint is also supported by K–Ar cooling ages of 550 ± 11 and 531 ± 11 Ma for nepheline and amphibole respectively, and a $^{206}Pb/^{238}U$ age of 494 ± 8 Ma for apatite from the alkaline rocks (Aftalion et al. 2000). These ages are broadly similar to the 487.1 ± 0.6 (2σ) and 499.0 ± 1.6 Ma (2σ) cooling ages obtained from two biotite-whole-rock isochrons in this study (Table 1). A Pan-African $^{207}Pb/^{206}Pb$ age of 593 Ma has also been
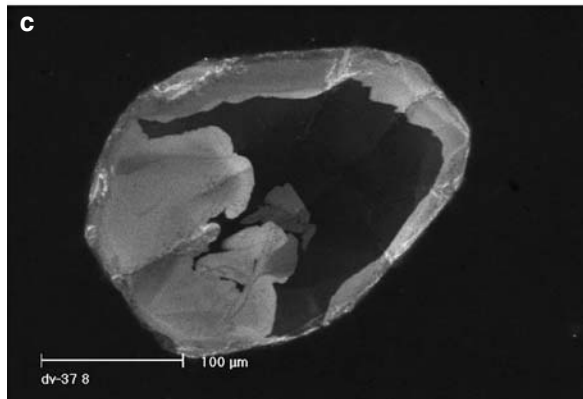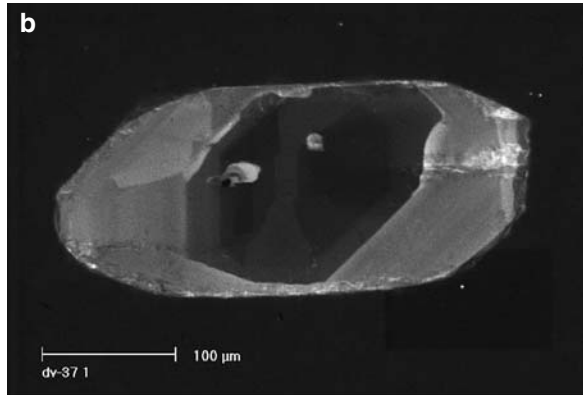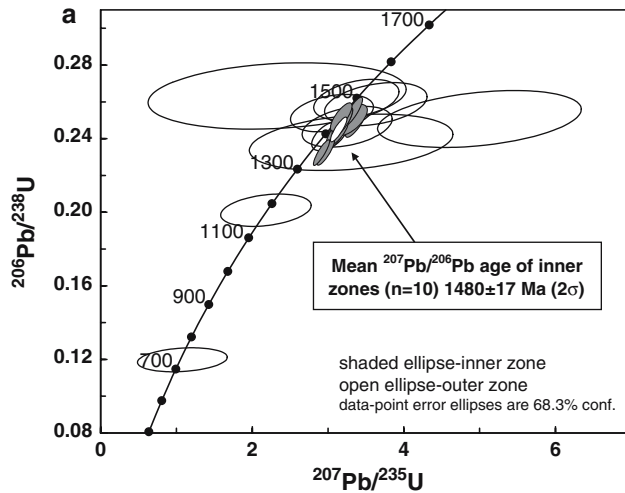
Fig. 3 a U–Pb concordia diagram illustrating the results of SHRIMP analyses on zircon grains from sample DU-37/2. The grain interiors give a mean $^{207}Pb/^{206}Pb$ age of $1,480 \pm 17$ Ma (2σ) which is interpreted as dating the emplacement of the Khariar alkaline rocks. The exteriors of the grains have low U–Th–Pb concentrations and high proportions of common Pb resulting in large uncertainties on the calculated ages. The discordance of the analyses may be due to disturbance in the U–Pb systematics during the Pan-African tectonothermal overprint. **b** and **c** Cathodoluminescence images of sectioned zircon grains showing their internal structures. Both grains have a comparatively poorly luminescent interior which is partially or totally enveloped by a more brightly luminescent exterior. Texturally, the luminescent exteriors can be grouped into two categories. In **b** the exterior shows weak concentric zones which follow the crystal faces of the interior regions while in **c** they truncate the internal zonation with a highly irregular boundary. Some grains have both kinds of exteriors where a concentrically zoned luminescent exterior and the darker interiors are truncated by a luminescent exterior having irregular boundary. See text for further discussion

migmatisation (Simmat 2003), while those in the mylonitic foliation wrapping around the garnets give Pan-African ages (472 ± 44 Ma, 2σ) and date the shear-related deformation associated with the thrusting of the EGP over the cratonic foreland.

Major and trace elements, Sr, Nd and Pb isotopic compositions

The major element concentrations show a large variation in the alkaline suite (Table 3). Most rocks have sodic affinities although the K_2O/Na_2O ratios vary between 0.3 and 3. The agpaitic index $[((Na_2O + K_2O)/Al_2O_3)_{molar}]$ has a narrow range (0.70–0.98) and reflects the miaskitic mineralogy of the rocks. Fe_2O_3 is chosen as a fractionation index in variation diagrams because (1) extremely low MgO concentrations (Table 3) make any Fe–Mg based index unreliable, (2) Fe concentrations are high and show a large variation in the suite (1–14 wt%), (3) a SiO_2 based differentiation index is unreliable because it is extremely sensitive to the ratio between nepheline and alkali feldspar which often occur as cumulus crystals in felsic alkaline rocks. On variation diagrams, Al_2O_3 and K_2O increase while CaO, TiO_2 and MgO decrease with decreasing Fe_2O_3 content, i.e. with increasing differentiation. Na_2O, SiO_2 (figure not shown) and P_2O_5 show scatter with general trends in which Na_2O and SiO_2 increase and P_2O_5 decreases with evolution (Fig. 5). The scatter in the P_2O_5 trend can be attributed to the presence of cumulus crystals of apatite in some samples. The major element trends indicate that the differentiation was dominated by the fractionation of ferromagnesian phases such as clinopyroxene and amphibole. This is also evident from the positive correlation between CaO–MgO and CaO–Fe_2O_3 (Figs. 5, 6). The CaO/Al_2O_3 ratio decreases with evolution implying the predominance of clinopyroxene in the fractionating assemblage (Fig. 5). The depletion of TiO_2 with differentiation and the positive correlation between CaO and

obtained from the TIMS analyses of titanites from the nepheline syenite sample DU-9/2 (data not presented).

The geological history of the EGP is in sharp contrast to that of the adjacent Khariar alkaline rocks. This is revealed from chemical dating of monazite grains in a garnet-sillimanite gneiss sample (DU-30/2) from the western margin of the EGP near to the contact with the Khariar alkaline complex. The results are listed in Table 2 and illustrated in Fig. 4. Two distinct textural varieties of monazites can be recognized which also define distinct age populations. The grains that occur as inclusions in leucosomal garnets furnish Grenvillian ages ($1,159 \pm 36$ Ma, 2σ) which may date the granulite-facies

Table 1 U–Th–Pb SHRIMP analyses of zircons (DU-37) and Rb–Sr isotopic ratios from biotite whole-rock pairs with isochron ages

Spot	Zone	U (ppm)	Th (ppm)	Th/U	Pb (ppm)	% com ^{206}Pb^{a}	^{207}Pb/^{206}Pb	±1σ	^{207}Pb/^{235}U	±1σ	^{206}Pb/^{238}U	±1σ	^{206}Pb/^{238}U Age (Ma)	±1σ	^{207}Pb/^{206}Pb Age (Ma)	±1σ
10b	Inner	129	137	1.06	40	0.54	0.0980	0.0015	3.367	0.091	0.2491	0.0051	1,434	26	1,587	28
9a	Inner	49	57	1.16	16	1.12	0.0956	0.0032	3.305	0.142	0.2507	0.0056	1,442	29	1,540	64
7b	Inner	172	306	1.78	62	0.41	0.0945	0.0013	3.329	0.084	0.2554	0.0051	1,466	26	1,518	25
8a	Inner	172	297	1.73	58	0.55	0.0932	0.0014	3.111	0.083	0.2421	0.0049	1,397	26	1,492	28
3b	Inner	131	126	0.97	39	0.53	0.0930	0.0013	3.203	0.083	0.2498	0.0051	1,437	26	1,488	26
10c	Inner	114	60	0.52	31	0.88	0.0929	0.0019	3.127	0.097	0.2441	0.0050	1,408	25	1,486	39
2b	Inner	302	546	1.81	106	0.23	0.0928	0.0006	3.205	0.068	0.2505	0.0049	1,441	26	1,484	13
1b	Inner	111	144	1.3	36	0.68	0.0928	0.0016	3.191	0.09	0.2495	0.0051	1,436	25	1,483	32
6a	Inner	128	159	1.24	38	0.51	0.0923	0.0013	2.972	0.078	0.2335	0.0048	1,353	25	1,474	27
3a	Inner	124	120	0.97	38	1.22	0.0912	0.0017	3.175	0.092	0.2525	0.0051	1,451	26	1,451	35
5a	Inner	190	253	1.33	57	0.57	0.0908	0.0010	2.917	0.069	0.2330	0.0046	1,350	24	1,442	21
5b	Outer	6	3	0.45	2	5.26	0.1446	0.0243	4.998	0.887	0.2507	0.0102	1,442	52	2,283	293
4a	Outer	14	4	0.32	4	3.06	0.1017	0.0118	3.630	0.446	0.2588	0.0077	1,484	40	1,656	216
8b	Outer	7	2	0.21	3	11.1	0.1007	0.0261	3.305	0.886	0.2380	0.0101	1,376	53	1,637	499
10a	Outer	13	16	1.19	5	4.81	0.0957	0.0108	3.252	0.392	0.2465	0.0073	1,420	38	1,542	214
7c	Outer	15	4	0.27	5	5.48	0.0937	0.0096	3.373	0.371	0.2612	0.0073	1,496	37	1,501	196
9c	Outer	53	8	0.14	13	1.86	0.0906	0.0039	3.018	0.154	0.2416	0.0054	1,395	28	1,438	82
1a	Outer	21	7	0.34	6	3.94	0.0872	0.0098	3.052	0.361	0.2539	0.0067	1,459	34	1,364	217
2a	Outer	17	10	0.61	4	5.83	0.0786	0.0137	2.181	0.394	0.2011	0.0058	1,181	31	1,163	352
7a	Outer	14	8	0.56	3	10.2	0.0653	0.0233	1.078	0.391	0.1198	0.0043	729	25	783	611
9b	Outer	7	2	0.23	3	16.7	0.0641	0.0305	2.328	1.124	0.2632	0.0119	1,506	61	746	774

Samp.	Desc.	Sr	Rb	^{87}Rb/^{86}Sr	^{87}Sr/^{86}Sr	±2σ	Age (Ma) ±2σ
1/3	Bt	8.60	1052	464	3.93865	0.000051	487.1±0.6
	W.R.	674	191	0.821	0.772698	0.000012	
14/2	Bt	28.5	1102	122	1.58954	0.000030	499±2
	W.R.	750	510	1.97	0.739270	0.000012	

^{a}Common Pb corrected using measured ^{204}Pb; *Bt* biotite, *W.R.* whole rock

Table 2 Results of electron microprobe dating of monazite from a garnet sillimanite gneiss

Spot	Zone	Th (ppm)	±2σ	U (ppm)	±2σ	Pb (ppm)	±2σ	Age (Ma)	Error[a]
4a core	In garnet	44,800	461	2,300	293	2,888	282	1,195	143
5a	In garnet	45,200	463	2,400	303	2,989	277	1,218	141
6a	In garnet	81,100	604	4,400	316	4,989	307	1,134	86
7a	In garnet	82,600	610	4,500	312	5,292	308	1,178	85
8a	In garnet	57,200	513	7,500	337	4,488	300	1,177	96
11b core	In garnet	48,200	475	5,900	325	3,789	287	1,203	112
12b	In garnet	47,100	470	6,300	328	3,693	289	1,169	112
13b	In garnet	45,000	462	6,400	330	3,780	286	1,224	114
14b	In garnet	46,100	467	6,900	331	3,583	291	1,120	110
15b	In garnet	45,400	462	6,800	331	3,482	290	1,106	111
16b	In garnet	45,300	462	6,900	329	3,382	283	1,072	108
2m core	In foliation	60,500	530	1,600	295	1,384	253	468	95
3m	In foliation	51,200	491	2,100	292	1,151	247	441	104
4m	In foliation	51,700	492	1,700	298	1,272	261	494	112
5m	In foliation	53,600	499	1,400	303	1,194	264	456	111
6m	In foliation	55,900	508	1,300	299	1,344	247	496	102
7m rim	In foliation	50,200	484	3,700	309	1,339	233	477	92

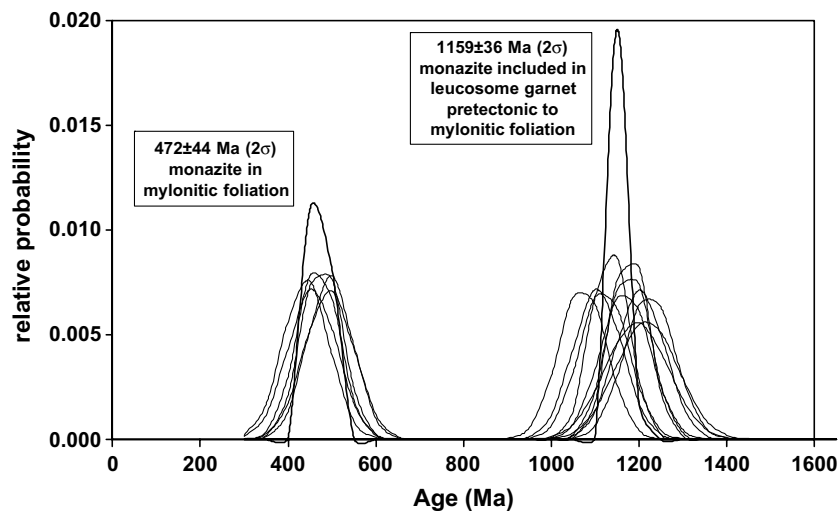[a]The errors on the ages represent 2σ

Fig. 4 Histogram showing the relative probability of U–Th–Pb EPMA ages from monazites in a garnet–sillimanite gneiss belonging to the EGP. Calculation of individual ages and age populations follows the procedure described in Montel et al. (1996). Monazite grains included in garnets of leucosomes that are pretectonic to the mylonitic foliation date the Grenvillian granu-lite-facies metamorphism and associated migmatisation in the EGP which may have been associated with the closure of the basin in which the EGP sedimentary units were deposited. Monazites occurring in the mylonitic foliation wrapping around the leuco-somes give distinct Pan-African ages which date the thrusting of the EGP over the craton

TiO$_2$ may be a result of titanite fractionation (Figs. 5, 6). Similarly, the decrease of P$_2$O$_5$ abundances with evolution and its positive correlation with CaO may be due to the fractionation of apatite (Figs. 5, 6). The incompatible behavior of K$_2$O, Na$_2$O and Al$_2$O$_3$ suggests that feldspar and biotite fractionation was minimal.

The rocks are enriched in the LIL elements including Rb (74–719 ppm), Sr (370–2,061 ppm) and Ba (158–3,377 ppm) which show a large variation in the suite. Except for the scatter caused by four samples, Ba abundances remain constant throughout the evolutionary history; the high concentrations in the four samples reflect the presence of cumulus feldspar and/or biotite (Fig. 7). In contrast, the concentrations of Rb show a ≈10 fold variation in the suite suggesting that it behaved as an extremely incompatible element during differentiation. However, the extremely high Rb concentration (719 ppm) of sample DU-35 may be due to the high modal abundance of biotite which is also seen in its spiked Ba concentration (969 ppm) (Fig. 7). The contrasting behavior of Ba and Rb indicates that biotite fractionation, if at all it had taken place, was minor. This is because high partition coefficients of biotite for Ba and Rb would deplete the melt in these elements. Since alkali feldspar has a preference for Ba ($D_{Ba}^{Kfs-melt} > 1$) relative to Rb ($D_{Rb}^{Kfs-melt} < 1$), minor fractionation of the phase could explain the incompatible behavior of Rb and the buffering of Ba concentrations.

Table 3 Representative major and trace element analyses of rocks from the Khariar alkaline complex

Sample	DU-1/5	DU-1/4	DU-1/1	DU-1/2	DU-1/3	DU-7	DU-9/1	DU-9/2	DU-9/3	DU-9/4a	DU-9/4b	DU-13/1
Rock	Ijolite	MNe–Sy	Ne–Sy	Ne–Sy	Ne–Sy	Ne–Sy	Ne–Sy	Ne–Sy	Ne–Sy	Ne–Sy	Ne–Sy	Ne–Sy
Major elements (wt. %)[a]												
SiO_2	45.97	47.55	53.06	58.08	56.83	56.37	55.93	53.80	54.51	53.98	50.15	53.02
TiO_2	0.89	1.83	0.59	0.24	0.33	0.26	0.45	0.59	0.14	0.42	0.10	0.44
Al_2O_3	15.99	13.77	21.68	20.79	22.28	22.21	21.63	20.95	22.85	22.36	26.73	24.11
Fe_2O_3	10.11	14.17	6.60	5.59	3.95	3.36	4.22	4.21	0.88	4.93	1.30	4.25
MnO	0.21	0.26	0.19	0.18	0.11	0.10	0.13	0.10	0.05	0.16	0.05	0.10
MgO	5.77	5.49	0.32	0.10	0.21	0.23	0.16	0.53	0.02	0.22	0.07	0.06
CaO	11.87	9.29	2.88	1.49	1.48	1.49	1.98	3.23	3.10	2.45	2.14	1.30
Na_2O	7.23	3.71	7.28	6.94	7.47	6.72	6.60	5.69	6.79	7.30	10.92	9.21
K_2O	2.11	3.45	6.70	6.89	7.72	8.92	8.95	9.48	9.57	8.31	7.24	7.51
P_2O_5	0.13	0.30	0.05	0.04	0.03	0.09	0.05	0.32	0.10	0.10	0.20	0.01
Total	100.4	100.1	99.6	100.6	100.6	100.0	100.4	99.46	98.04	100.4	99.04	100.2
Trace elements (ppm)												
Li	NA	6.00	7.00	2.00	5.70	NA	NA	5.70	NA	NA	NA	NA
Be	NA	6.60	3.40	4.90	2.40	NA	NA	4.70	NA	NA	NA	NA
Sc	NA	36.0	1.80	0.45	1.10	NA	NA	2.60	NA	NA	NA	NA
V	NA	277	6.02	2.65	4.28	NA	NA	18.0	NA	NA	NA	NA
Cr	NA	77.1	7.14	9.06	7.67	NA	NA	9.36	NA	NA	NA	NA
Co	NA	46.0	4.00	1.00	1.70	NA	NA	4.50	NA	NA	NA	NA
Ni	NA	62.0	22.0	27.0	23.0	NA	NA	26.0	NA	NA	NA	NA
Cu	NA	24.0	5.00	2.00	4.40	NA	NA	9.70	NA	NA	NA	NA
Zn	NA	145	91.5	142	62.9	NA	NA	85.2	NA	NA	NA	NA
Ga	NA	21.0	34.0	40.0	28.0	NA	NA	28.0	NA	NA	NA	NA
Rb	NA	74.0	161	209	191	NA	NA	351	NA	NA	NA	NA
Sr	NA	329	966	493	674	NA	NA	1724	NA	NA	NA	NA
Y	NA	49.0	32.0	16.0	11.0	NA	NA	24.0	NA	NA	NA	NA
Zr	NA	162	235	239	138	NA	NA	203	NA	NA	NA	NA
Nb	NA	36.0	125	308	63.0	NA	NA	112	NA	NA	NA	NA
Cs	NA	0.10	0.45	0.42	0.38	NA	NA	1.60	NA	NA	NA	NA
Ba	NA	514	366	158	383	NA	NA	2368	NA	NA	NA	NA
La	NA	76.0	65.0	111	13.8	NA	NA	80.0	NA	NA	NA	NA
Ce	NA	166	179	214	36.8	NA	NA	166	NA	NA	NA	NA
Pr	NA	20.0	27.0	22.0	5.60	NA	NA	19.0	NA	NA	NA	NA
Nd	NA	84.0	140	72.0	24.4	NA	NA	67.0	NA	NA	NA	NA
Sm	NA	15.0	26.9	9.9	4.4	NA	NA	10.2	NA	NA	NA	NA
Eu	NA	4.10	8.10	1.20	1.46	NA	NA	1.80	NA	NA	NA	NA
Gd	NA	13.0	21.0	6.40	3.30	NA	NA	7.40	NA	NA	NA	NA
Tb	NA	1.88	3.10	0.88	0.48	NA	NA	ND	NA	NA	NA	NA
Dy	NA	9.40	10.0	4.20	2.17	NA	NA	5.00	NA	NA	NA	NA
Ho	NA	1.70	1.60	ND	0.39	NA	NA	0.99	NA	NA	NA	NA
Er	NA	4.70	3.20	2.30	0.91	NA	NA	2.40	NA	NA	NA	NA
Tm	NA	0.62	0.41	ND	0.12	NA	NA	0.30	NA	NA	NA	NA
Yb	NA	4.00	2.50	2.30	0.74	NA	NA	1.90	NA	NA	NA	NA
Lu	NA	0.63	0.41	0.39	0.14	NA	NA	0.27	NA	NA	NA	NA
Hf	NA	3.87	7.99	8.68	4.74	NA	NA	5.92	NA	NA	NA	NA
Ta	NA	1.54	6.60	23.5	3.00	NA	NA	7.70	NA	NA	NA	NA
Pb	NA	4.57	7.90	11.3	8.20	NA	NA	7.10	NA	NA	NA	NA
Th	NA	5.26	4.10	14.0	0.61	NA	NA	13.8	NA	NA	NA	NA
U	NA	1.35	0.50	17.2	0.12	NA	NA	3.10	NA	NA	NA	NA

Sample	DU-13/2	DU-14/2	DU-15/1	DU-15/2	DU-24	DU-35	DU-36	DU-43	DU-17	DU-48	DU-39	JB-3
Rock	Ne-Sy	Ne-Sy	Ne-Sy	Ne-Sy	Ne-Sy	Ne-Sy	Ne-Sy	Ne-Sy	Thol.	B-Gr	A-Gr	Basalt +
Major elements (wt. %)*												
SiO_2	54.59	55.63	56.64	54.50	54.59	55.55	48.14	59.11	48.58	71.77	68.45	NA
TiO_2	0.61	0.14	0.14	0.52	0.35	0.21	0.68	0.79	1.61	0.10	0.23	NA
Al_2O_3	19.80	23.14	23.38	20.28	21.25	22.74	18.96	17.79	13.65	15.72	15.64	NA
Fe_2O_3	7.84	1.05	1.54	6.84	5.83	1.44	6.15	7.39	15.06	0.46	1.98	NA
MnO	0.24	0.02	0.04	0.20	0.25	0.03	0.17	0.19	0.23	0.01	0.04	NA
MgO	0.21	0.03	0.05	0.13	0.24	0.11	0.12	0.64	7.04	0.18	0.66	NA
CaO	3.30	0.73	0.81	2.99	2.34	0.60	3.13	3.54	11.80	1.22	3.20	NA
Na_2O	6.33	5.91	7.83	6.39	7.37	6.02	5.42	5.44	2.17	4.79	6.13	NA
K_2O	7.33	13.35	9.24	8.12	7.58	13.44	7.59	5.10	0.16	4.89	2.39	NA
P_2O_5	0.03	0.06	0.01	0.06	0.08	0.06	0.05	0.25	0.14	0.02	0.08	NA
Total	100.6	100.1	99.90	100.3	99.89	100.2	90.74	100.6	100.5	99.51	99.02	

Table 3 (Contd.)

Sample Rock	DU-13/2 Ne-Sy	DU-14/2 Ne-Sy	DU-15/1 Ne-Sy	DU-15/2 Ne-Sy	DU-24 Ne-Sy	DU-35 Ne-Sy	DU-36 Ne-Sy	DU-43 Ne-Sy	DU-17 Thol.	DU-48 B-Gr	DU-39 A-Gr	JB-3 Basalt +
Trace elements (ppm)												
Li	1.30	1.60	1.20	NA	3.40	1.60	4.30	2.60	10.15	4.05	5.80	7.51
Be	1.04	1.42	0.83	NA	0.93	0.53	0.37	5.20	0.52	1.05	4.25	NA
Sc	0.90	0.18	0.50	NA	0.94	0.42	0.48	3.90	40	0.91	2.63	34
V	2.16	3.69	1.58	NA	2.58	3.28	0.30	2.29	320	4.32	11.4	NA
Cr	6.70	4.53	9.99	NA	4.65	6.66	7.42	5.21	116	14.7	22.5	NA
Co	3.00	0.51	0.60	NA	1.79	0.90	2.20	4.00	48.0	0.80	3.91	37.3
Ni	22.0	15.0	32.0	NA	19.7	14.0	24.0	18.0	74.2	48.7	58.0	41.5
Cu	7.00	1.00	2.00	NA	2.80	2.00	17.0	12.0	5.83	0.33	0.12	193
Zn	74.0	9.37	11.4	NA	65.9	16.3	41.5	116	78.3	3.5	31.7	NA
Ga	30.0	23.0	35.0	NA	36.0	23.0	27.0	30.0	15.1	12.4	14.5	20.6
Rb	153	532	208	NA	221	719	133	122	4.0	82	68	16.3
Sr	1344	752	1146	NA	415	561	2061	644	160	869	612	395
Y	10.0	1.5	4.20	NA	27.0	1.8	3.5	53.0	25.4	1.2	25.4	25.0
Zr	200	3.28	61.6	NA	254	2.26	164	194	20.7	41.7	64.9	NA
Nb	34.0	12.1	16.0	NA	397	22.0	14.4	164	4.71	2.16	6.18	2.07
Cs	0.18	3.20	0.22	NA	0.32	3.40	0.06	0.16	ND	0.14	0.52	0.92
Ba	376	3377	307	NA	275	970	308	2708	33	3734	1150	NA
La	20.0	7.90	8.90	NA	219	9.50	13.5	135	5.51	9.29	65.2	8.50
Ce	58.0	12.0	21.3	NA	389	18.0	40.2	255	12.9	12.7	113	21.0
Pr	9.10	ND	2.80	NA	37.8	2.00	6.78	31.0	2.09	1.29	14.2	3.50
Nd	44.0	5.60	11.7	NA	139	8.00	31.8	118	10.9	4.18	61.7	16.0
Sm	8.05	1.16	2.13	NA	21.3	1.66	5.55	21.0	3.20	0.67	10.2	4.30
Eu	3.00	0.28	1.12	NA	4.00	0.40	2.34	5.00	0.99	0.86	2.54	1.30
Gd	5.30	0.67	1.61	NA	15.2	0.87	3.51	16.0	3.75	0.52	7.92	4.50
Tb	ND	ND	0.23	NA	1.98	ND	0.35	2.10	0.78	0.05	1.03	0.84
Dy	2.90	0.34	1.02	NA	7.71	0.47	1.25	11.0	4.47	0.19	4.76	4.50
Ho	0.50	0.06	0.17	NA	1.26	0.07	0.17	2.20	0.98	0.04	0.83	0.89
Er	1.30	0.12	0.44	NA	3.04	0.15	0.45	5.50	2.89	0.13	2.11	2.70
Tm	0.20	ND	0.07	NA	0.38	ND	0.08	0.73	0.41	0.02	0.27	0.37
Yb	2.00	0.08	0.54	NA	3.11	0.10	0.78	4.70	2.56	0.11	1.55	2.50
Lu	0.43	0.01	0.11	NA	0.50	0.01	0.19	0.72	0.37	0.02	0.19	0.39
Hf	5.82	0.08	1.94	NA	11.4	0.07	3.38	5.36	0.92	1.23	2.04	NA
Ta	2.50	0.47	1.00	NA	26.0	0.89	2.60	9.00	0.32	0.06	0.29	0.19
Pb	1.60	1.10	2.50	NA	3.06	2.10	2.30	11.5	1.34	57.5	41.2	4.83
Th	0.53	0.53	0.59	NA	18.6	1.20	0.35	11.6	0.39	2.32	26.9	1.20
U	0.11	0.12	0.09	NA	5.05	0.12	0.05	1.55	0.09	0.39	2.16	0.47

Ne–Sy Nepheline syenite, *Thol.* Tholeiite, *B-Gr* Basement granite, *A-Gr* Alkali granite,
+ international rock standard (Govindaraju 1994), *MNe-Sy* Mesocratic nepheline syenite, *Ne-Sy* Nepheline syenite *NA* not analyzed; *ND*
not detected
[a]Anhydrous concentrations

Rb also shows a positive correlation with K_2O (figure not shown) which further supports the inference that it was relatively incompatible in most of the fractionating phases. Sr concentrations show a large scatter which may be due to the presence of cumulus alkali feldspar.

On the basis of the REE and other incompatible elements, the alkaline rocks can be divided into two groups: (1) nepheline syenites that have cumulus crystals of allanite, titanite and apatite and (2) cumulus phase-free nepheline syenites. The cumulus phase-free rocks show coherent variations of the trace element concentrations and define a differentiation series with the mesocratic nepheline syenite as the most primitive member (Fig. 7). The nepheline syenites in this group show trends in which Fe, Mg, Ti, Sc, Zr and REE concentrations decrease with differentiation indicating that fractional crystallization was dominated by clinopyroxene, amphibole and accessory phases which host bulk of the REE in such evolved alkaline systems

(Fig. 7). Figures 8a, b illustrate the chondrite- and mesocratic nepheline syenite-normalized REE patterns of the cumulus phase-free nepheline syenites in which the depletion of the REE can be correlated with increasing differentiation. Starting with a straight REE pattern for the most primitive sample (DU-1/4), the LREE and MREE were progressively depleted giving rise to patterns which are convex and concave upward at the LREE and MREE respectively. The LREE depletion can be explained by allanite fractionation, an abundant accessory phase in many of the nepheline syenites, while the MREE depletion is a combined result of titanite and apatite fractionation. The most evolved samples (DU-35 and DU-14/2) show a strong depletion of the HREE which is correlatable with low Zr and Hf concentrations and is indicative of greater modal proportions of zircon in the fractionating assemblage during the later stages of melt evolution (Figs. 8a, b; 9). The absence of any significant negative Eu anomaly in most
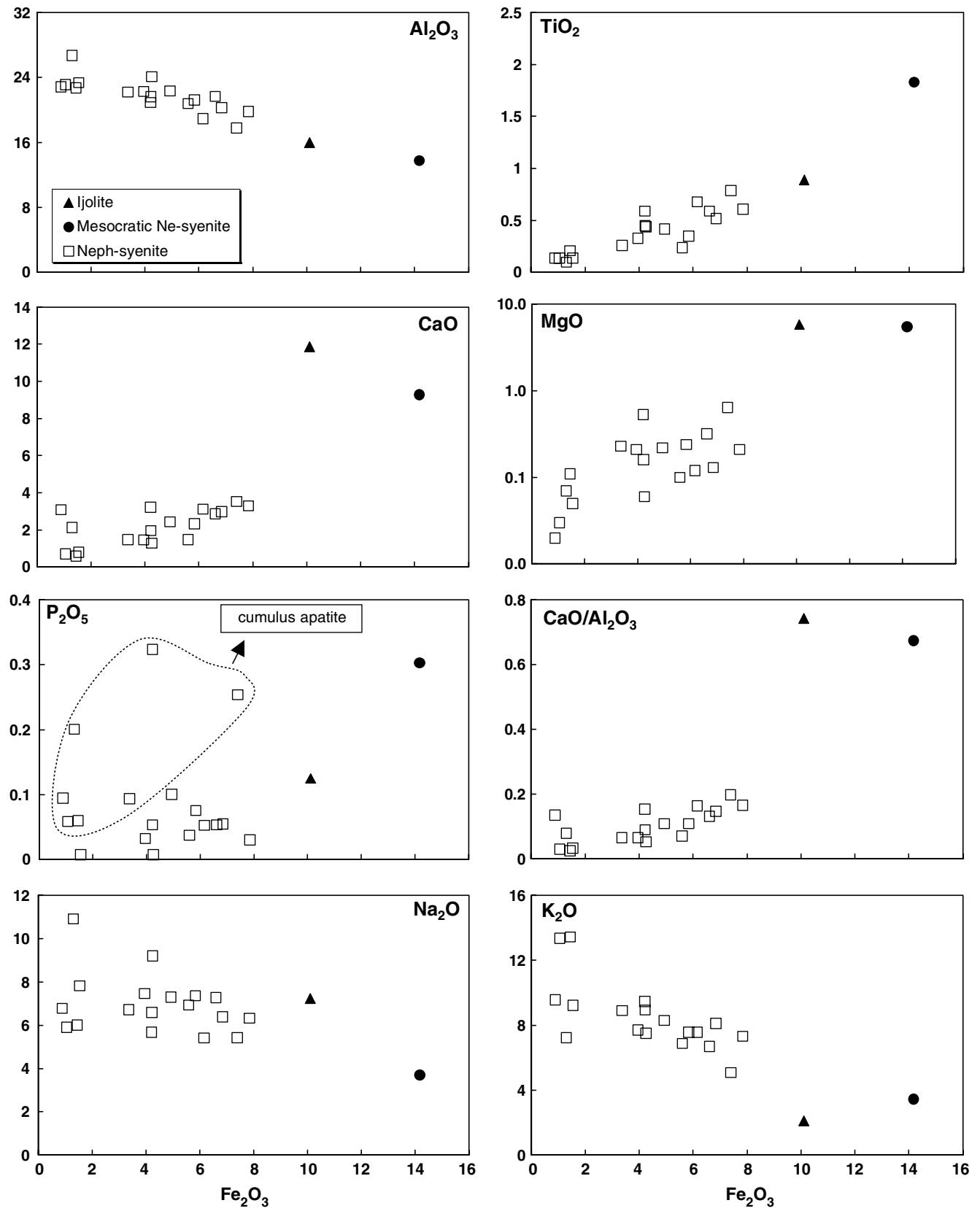
Fig. 5 Bivariate plots showing the trends of major element concentrations for the Khariar alkaline series
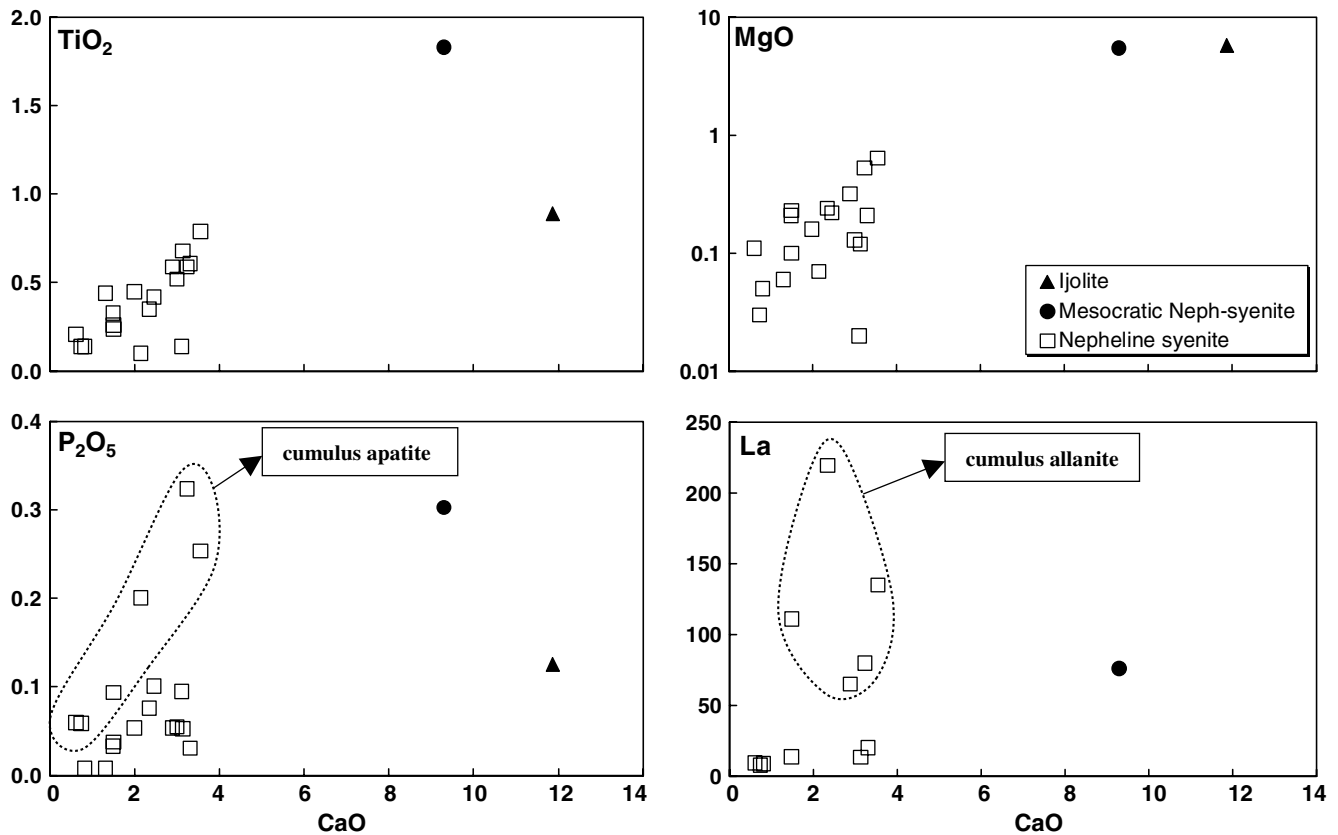
Fig. 6 Bivariate plots of selected elements against CaO concentrations for the Khariar alkaline rocks

samples indicates that feldspar fractionation was minimal. Figure 9a shows the primitive mantle-normalized multi-element patterns for the cumulus phase-free rocks, with the positive Nb anomalies suggesting a rift-related tectonic setting for the alkaline magmatism. The variations seen in the multi-element diagram reflect evolutionary trends in which Cs, Th, U, REE, Zr, Hf, Ti and Y concentrations decrease and Rb, K and Sr concentrations increase with differentiation. In summary, the geochemical variations in this group can be explained by a fractional crystallization scheme dominated by the removal of clinopyroxene, amphibole and minor amounts of allanite, zircon, titanite and apatite which can collectively account for the decrease in Fe, Mg, and Ti and trace elements like the REE, U, Th, Zr, Hf and Y. Biotite and alkali feldspar were insignificant as fractionating phases.

The idea of a differentiation scheme involving the fractionation of accessory phases such as allanite, apatite and titanite is supported by the presence of these phases as cumulus crystals in some nepheline syenites. Such samples represent variably evolved liquids with the only distinction that they are enriched in the REE in general and the LREE and the MREE in particular in comparison to similarly evolved nepheline syenites of the cumulus phase-free group (Fig. 9c). The LREE and MREE enrichment in these rocks is also evident in multi-element diagrams (Fig. 9b) and the REE patterns

normalized to a similarly evolved nepheline syenite of the cumulus phase-free group (Fig. 8d). The spike in the LREE and MREE concentrations correlates with the high modal abundances of allanite, titanite and apatite in these rocks indicating that these were cumulus phases.

The nepheline syenites have moderately radiogenic initial $^{87}Sr/^{86}Sr$ ratios (0.7031–0.7041; ε_{iSr} = −11.3 to 3; DePaolo 1988), low $^{143}Nd/^{144}Nd$ ratios (0.510645–0.510691; ε_{iNd} = −1.6 to −0.7; Wasserburg et al. 1981), and plot in the enriched quadrant of the Sr-Nd diagram (Table 4, Fig. 10). The isotopic ratios are distinctly less radiogenic than those of the host basement granites implying that the cratonic crust was not the source region for the alkaline magma. Although the enriched Sr–Nd isotopic ratio of the least radiogenic nepheline syenite can be explained by about 25–30% contamination of a DM-derived MORB-like magma by a crustal source similar to the cratonic basement granite, the resultant melt would be relatively silicic (55 wt.% SiO_2) which is contrary to the low SiO_2 content (47.5 wt.%) of the most primitive sample (DU-1/4). Moreover, the Sr and Nd isotopes do not define any two component mixing relationships on plots of initial $^{87}Sr/^{86}Sr$ against 1/Sr or $^{143}Nd/^{144}Nd$ against 1/Nd, nor do they show any positive correlation with SiO_2, which indicates that AFC processes (DePaolo 1981) or crustal contamination did not play a significant role in their evolution. The isotopic ratios may consequently reflect the characteristics of the
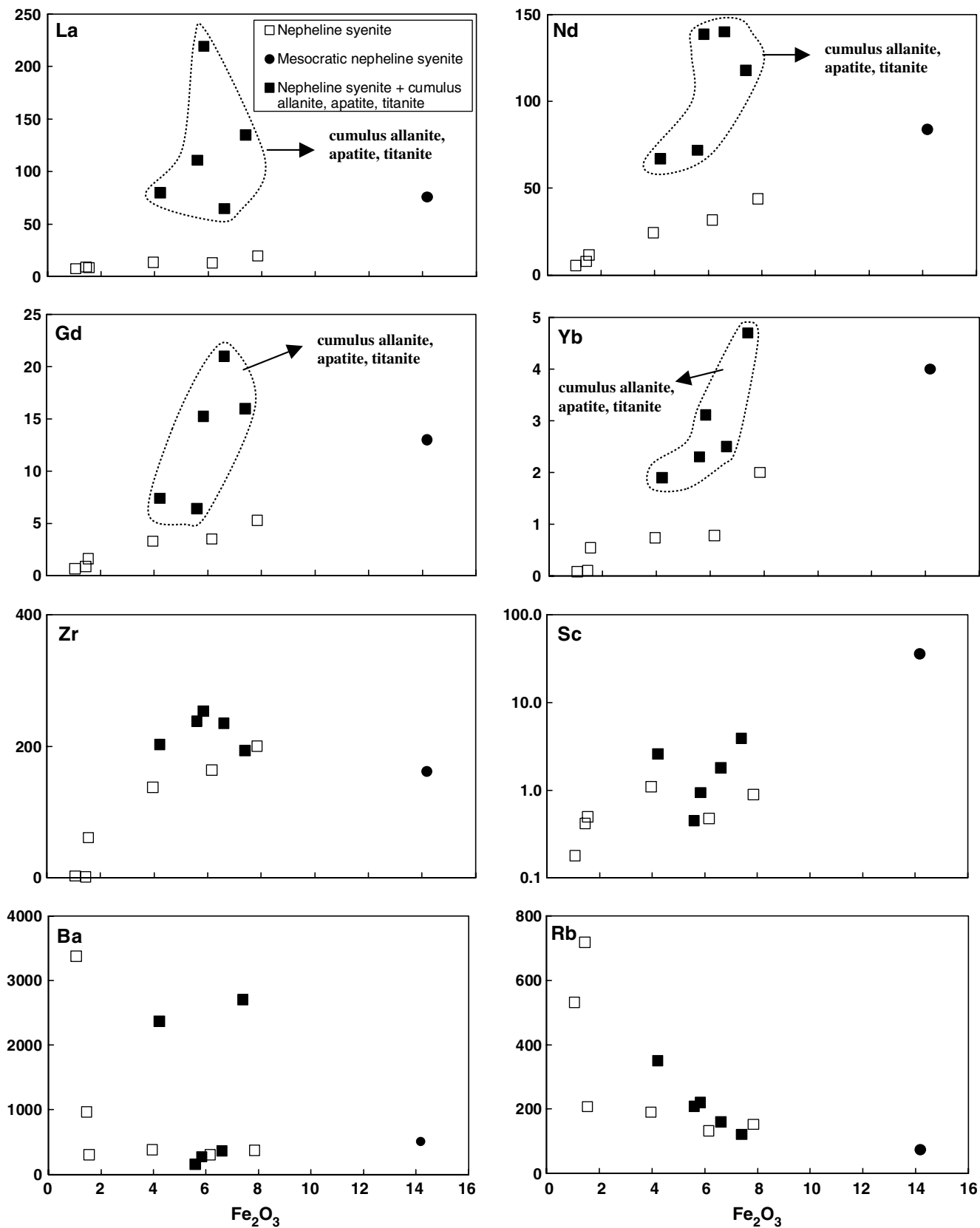
Fig. 7 Variation diagrams showing the trends of the trace element concentrations with differentiation in the Khariar alkaline series
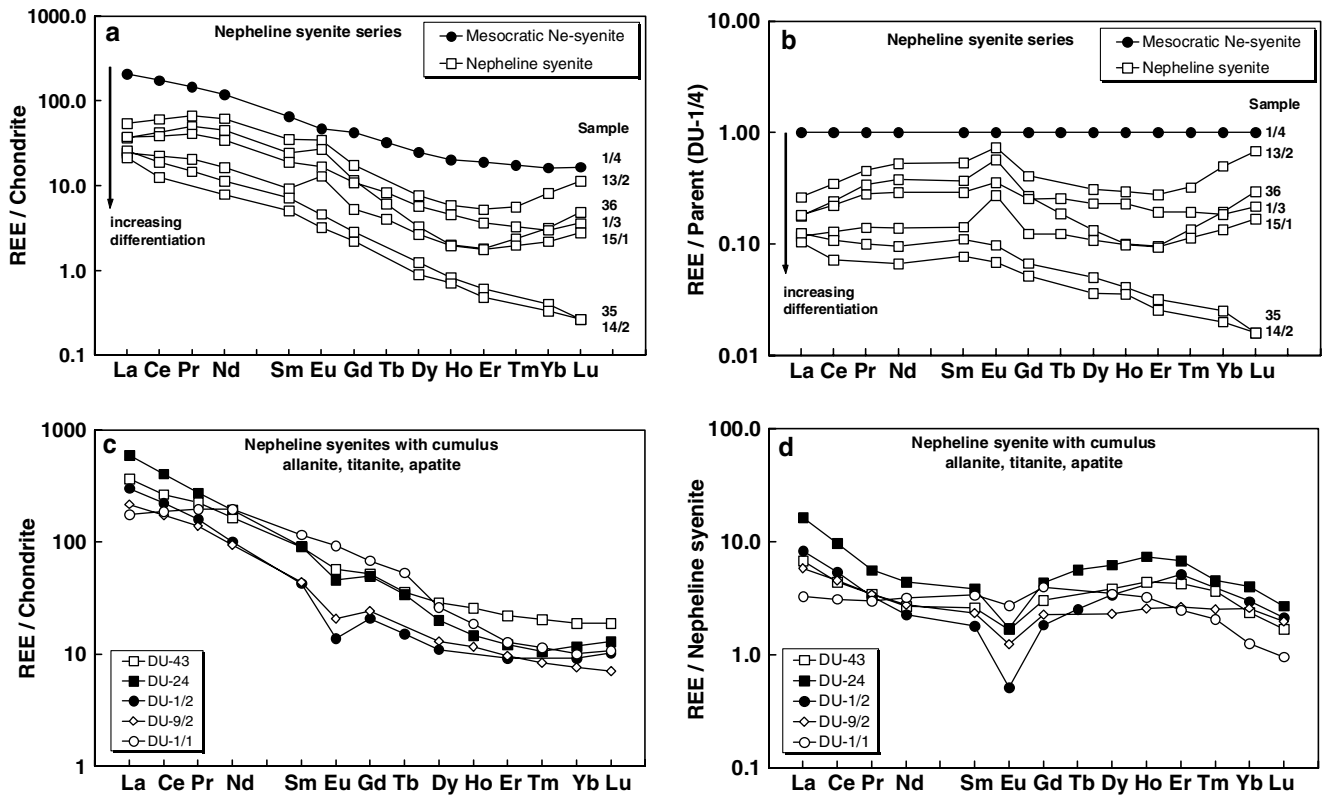
Fig. 8 a and **b** Chondrite- and parent melt (mesocratic nepheline syenite, DU-1/4)-normalized REE patterns of the cumulus phase-free nepheline syenite group which define a coherent variation of the major and trace element concentrations. **c** Chondrite-normalized REE patterns of nepheline syenites having cumulus crystals of apatite, titanite and allanite. **d** REE patterns of the cumulus phase-bearing nepheline syenites normalized to a cumulate phase-free nepheline syenite having similar #Mg, i.e. similarly evolved. The patterns are characteristically enriched in the LREE and MREE which confirms petrographic observations that some allanite, titanite and apatite may be cumulus. The normalizing values are from Taylor and McLennan (1985)

source region rather than any significant contamination. The initial Pb isotopic ratios from five of the six leached feldspar separates measured are characterized by relatively high $^{207}Pb/^{204}Pb$ (15.90–16.15) and 'normal' $^{208}Pb/^{204}Pb$ (39.66–40.50) for the measured $^{206}Pb/^{204}Pb$ ratios (18.85–19.46) (Table 4; Fig. 11). One sample is distinctly more radiogenic and has a high $^{206}Pb/^{204}Pb$ ratio (23.34). The isotopic ratios are significantly more radiogenic than those of the cratonic crust (Rickers et al. 2001) which further indicates that the alkaline magma was not derived from a crustal source (Fig. 11). The high $^{207}Pb/^{204}Pb$ and $^{206}Pb/^{204}Pb$ ratios require a source which had evolved with a high U/Pb value at least sometime prior to the extraction of the alkaline magma. However, the 'normal' $^{208}Pb/^{204}Pb$ suggests that the Th/Pb and the Th/U ratios of the source had remained constant.

The granite forming the cratonic basement has typical crustal $^{87}Sr/^{86}Sr$ (0.7054) and ε_{Nd} (−11.6) values at 1,480 Ma (Table 4, Fig. 10) with a DM Nd model age of ≈2.6 Ga. The alkali granite in contrast has a strongly radiogenic $^{87}Sr/^{86}Sr$ (0.7088), but a younger model age (2.0 Ga) and higher ε_{Nd} (−2.2), similar to those of the nepheline syenites. Thus, the alkali granite body is distinctly different from the older basement granite gneisses and probably represents a younger intrusive related to the rift activity.

Discussion

Source region of the alkaline magma

Compositionally, the most primitive cumulus phase-free rock (i.e. the mesocratic nepheline syenite, DU−1/4) could represent the parent magma for the nepheline syenites. Such a parent having low #Mg (≈43) and accompanying depletion of Ni (62 ppm), Cr (77 ppm), Sc (36 ppm) and other compatible trace elements must itself represent an evolved product of a more primitive primary magma. Its high Nb/Ta (23.3), Zr/Hf (41.8) and mantle-like Th/U ratio (3.9) indicate that it could not have been derived from a crustal source (Nb/Ta of the crust is ≈12). Hence, the source region for the melt must have been an enriched mantle domain.

The radiogenic Sr and low Nd isotopic ratios of the alkaline rocks are also indicative of an enriched mantle source which had significant incubation time prior to the extraction of the alkaline magma. The high Nb/Ta ratios suggest that such a mantle could have been a part of the

Fig. 9 a and **b** Primitive mantle normalized multi-element diagrams for the cumulus phase-free and cumulus phase-bearing nepheline syenites respectively. The positive Nb–Ta anomalies suggest a rift/hotspot related tectonic setting for the alkaline rocks. The cumulus phase-free nepheline syenites show trends in which Cs, Th, U, REE, Zr, Hf, Ti and Y concentrations decrease while Rb, K and Sr concentrations increase with differentiation. The cumulus phase-bearing nepheline syenites are enriched in the REE in general and the LREE and MREE in particular which supports the interpretation that they have cumulus crystals of allanite, apatite and titanite. The normalizing values are from Taylor and McLennan (1985)
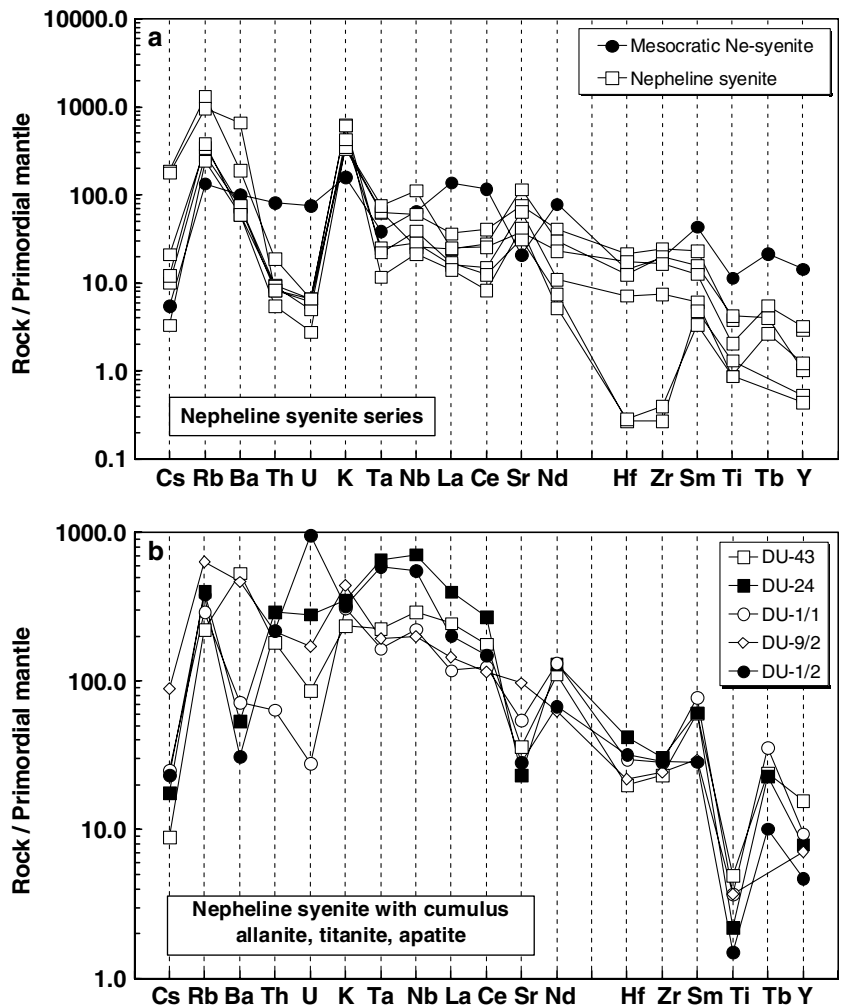
sub-continental lithosphere (Münker et al. 2003). The variation in the Pb isotope ratios of the alkali feldspars (Fig. 11) may be attributed to heterogeneity in the source magma or incomplete removal of the radiogenic Pb during leaching. It is unlikely to be an effect of mixing between different sources or magmas because (1) no mixing relationship is observed for the Sr–Nd isotopes, (2) if the linear array defined by the Pb isotopes represent a mixing line, the more radiogenic end member would have had extremely radiogenic ratios which is difficult to envisage for the Proterozoic crust or mantle. The ratios hence could either define an 'isochron' showing a heterogeneous evolution of the source or reflect the incorporation of radiogenic lead during the metamorphic overprint (Fig. 11). If the feldspars are not leached enough, they would move down along the linear array or along a line parallel to the linear array for the two samples with high $^{207}Pb/^{204}Pb$ with further leaching. In all possible cases, the $^{207}Pb/^{204}Pb$ ratios would be distinctly high and could never end up near one of the mantle reservoirs or the Bhandara cratonic crust. For this reason, the alkaline parent melt could not have been derived directly from any of these sources. Moreover, the cratonic crust has much lower $^{207}Pb/^{204}Pb$ ratios and

contamination of the alkaline magma by such a component would actually lower its Pb isotope ratios. Hence, it can be argued that the high $^{207}Pb/^{204}Pb$ ratios are a characteristic of the source which had evolved with a high U/Pb ratio, rather than an effect of crustal assimilation. A line joining the Pb data cluster with the ≈1.5 Ga (intrusion age of the alkaline rocks) point on the Stacey and Kramers (1975) curve, if projected backward, also cuts the curve at about 2.0 Ga which is similar to the DM model ages (Goldstein et al. 1984) (1.9–2.1 Ga) of the rocks. The enrichment of the lithospheric mantle and the concomitant deviation of the U/Pb ratio from the Stacey and Kramers (1975) curve could thus have occurred at about 1.9–2.1 Ga. The source, enriched in Rb and U relative to Pb, then evolved until 1.5 Ga which gave it sufficient incubation time to generate the moderately radiogenic Sr–Nd isotopic ratios and the high $^{207}Pb/^{204}Pb$ at the time of the alkaline magma extraction.

The $^{143}Nd/^{144}Nd$ ratio of the alkali granite is similar to those of the nepheline syenites and distinctly higher than that of the adjacent cratonic crust at 1,480 Ma. It therefore could not have been derived from any crustal source similar to the exposed cratonic basement. Rather,

Table 4 Rb-Sr, Sm-Nd and Pb isotopic data of studied samples

Sr-Nd		Rb (ppm)	Sr (ppm)	Sm (ppm)	Nd (ppm)	$^{87}Rb/^{86}Sr$	$^{87}Sr/^{86}Sr$	2σ mean	$^{147}Sm/^{144}Nd$	$^{143}Nd/^{144}Nd$	2σ mean	$^{87}Sr/^{86}Sr$ (1480 Ma)	$^{143}Nd/^{144}Nd$ (1480 Ma)	[a]ε_{Nd}	T_{DM} (Ma) +
DU-1/1	Ne–Sy	161	966	26.9	140	0.482	0.713851	0.000010	0.1162	0.511789	0.000004	0.703604	0.510659	-1.3	2065
DU-1/2	Ne–Sy	209	493	9.90	72.0	1.229	0.730001	0.000013	0.08310	0.511481	0.000005	0.703894	0.510673	-1.0	1905
DU-1/3	Ne–Sy	191	674	4.37	24.4	0.821	0.720698	0.000012	0.10805	0.511701	0.000006	0.703262	0.510650	-1.5	2034
DU-1/4	MNe–Sy	74	329	15.0	84.0	0.651	0.717876	0.000011	0.1079	0.511706	0.000005	0.704041	0.510656	-1.4	2025
DU-9/2	Ne–Sy	351	1724	10.2	67.0	0.590	0.716274	0.000017	0.09228	0.511580	0.000005	0.703753	0.510682	-0.8	1925
DU-9/3	Ne–Sy	363	1659	4.40	27.9	0.634	0.716547	0.000011	0.09499	0.511600	0.000005	0.703090	0.510676	-1.0	1942
DU-13/2	Ne–Sy	153	1344	8.05	44.0	0.329	0.711092	0.000013	0.1106	0.511737	0.000005	0.704095	0.510662	-1.2	2031
DU-15/1	Ne–Sy	208	1146	2.13	11.7	0.525	0.714363	0.000013	0.1103	0.511735	0.000005	0.703203	0.510662	-1.2	2030
DU-24	Ne–Sy	221	405	21.3	139	1.583	0.737056	0.000011	0.09265	0.511592	0.000005	0.703428	0.510691	-0.7	1916
DU-36	Ne–Sy	133	2061	5.55	31.8	0.187	0.707516	0.000013	0.1053	0.511669	0.000005	0.703551	0.510645	-1.6	2028
DU-37	Ne–Sy	120	842	1.40	7.10	0.413	0.712700	0.000013	0.1192	0.511829	0.000005	0.703938	0.510670	-1.1	2066
DU-43	Ne–Sy	122	644	21.0	118	0.548	0.715086	0.000013	0.1076	0.511732	0.000005	0.703437	0.510686	-0.8	1982
DU-17	Thol.	4.0	160	3.20	10.9	0.072	0.703187	0.000013	0.1773	0.512811	0.000006	0.701652	0.511087	7.1	1338
DU-48	B–Gr	82	869	0.67	4.18	0.273	0.711224	0.000012	0.09687	0.511077	0.000017	0.705424	0.510135	-12	2628
DU-39	A–Gr	68	532	10.2	61.7	0.370	0.716674	0.000014	0.09956	0.511582	0.000005	0.708813	0.510614	-2.2	2041

Pb		$^{206}Pb/^{204}Pb$	2 σ%	$^{207}Pb/^{204}Pb$	2 σ%	$^{208}Pb/^{204}Pb$	2 σ%
DU-1/1	Ne–Sy	19.07	0.03	15.91	0.03	39.94	0.03
DU-1/2	Ne–Sy	23.34	0.09	16.26	0.11	40.51	0.11
DU-1/3	Ne–Sy	18.85	0.03	15.90	0.03	39.66	0.03
DU-9/2	Ne–Sy	19.46	0.07	15.94	0.07	40.48	0.07
DU-13/2	Ne–Sy	19.37	0.13	16.01	0.13	40.50	0.13
DU-37	Ne–Sy	19.37	0.10	16.15	0.10	40.19	0.10

Abbreviations same as in Table 3

[a] ε_{Nd} values calculated at 1,480 Ma; + DM model ages after Goldstein et al. (1984)

Fig. 10 Initial Sr-Nd isotopic ratios of the nepheline syenites, alkali granite and the basement granite. Also shown in the figure are the approximate positions of the other important mantle reservoirs at 1,480 Ma: depleted mantle, DM (Goldstein et al. 1984), Bulk Earth/Chondrite (CHUR, DePaolo 1988; Wasserburg et al. 1981) and enriched mantle (*EM*, enriched mantle calculated back using the present day isotopic ratios from EM-I, Rehkämper and Hofmann 1997). The alkaline rocks define a relatively narrow field in the enriched quadrant
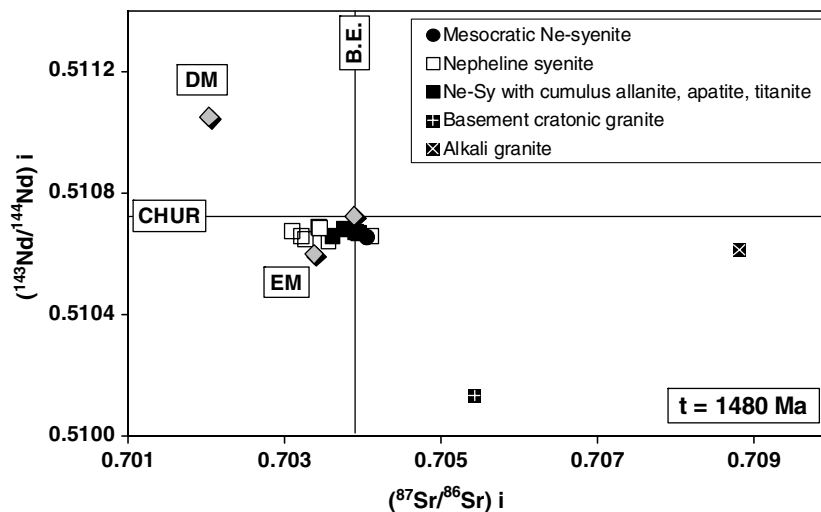
its alkaline nature suggests a genetic link with the nepheline syenites. However, a thermal barrier in the nepheline–albite–quartz system prevents the formation of simultaneous undersaturated and oversaturated magmas from the same source by partial melting or fractional crystallization. It may thus have formed by the contamination of the undersaturated alkaline magma with a crustal component having high Rb/Sr ratios and radiogenic $^{87}Sr/^{86}Sr$ different from the basement granites. Alternatively, the high $^{87}Sr/^{86}Sr$ ratio may be due to the decoupling of Rb from Sr during the Pan-African metamorphic overprint.

Differentiation of the parent nepheline syenite magma

The major and trace element variations in the cumulus phase-free nepheline syenites require a fractional crystallization mechanism which must be able to account for the following observations: (a) the depletion of Fe and Mg with differentiation was accompanied by a simultaneous decrease in the compatible and 'incompatible' trace element concentrations which requires high bulk mineral-melt partition coefficients (D) for the fractionating assemblage. Since the bulk of the 'incompatible' trace elements are hosted in the accessory phases allanite, titanite, apatite and zircon, the fractionation of ferromagnesian phases such as clinopyroxene and amphibole must have been coupled with the removal of the accessory phases as well; (b) The changing geometry of the REE patterns correlated with magmatic evolutionary trends suggests that the initial stages of differentiation involved removal of allanite, titanite and apatite that can account for the depletion of the LREE and MREE. The later stages of the evolution however, involved substantial decrease in the HREE abundances but smaller decrease in the LREE and MREE. This is consistent with fractionation of zircon together with lesser amounts of allanite, apatite and titanite.

The mesocratic nepheline syenite sample (DU-1/4) which is the most primitive member of the suite is inferred to approximate the composition of the parent magma for the nepheline syenites. The differentiation from such a parent to the most evolved nepheline syenite requires the removal of more than 90% of the bulk Fe_2O_3 and also leads to about seven times enrichment in the Rb concentrations (excluding sample DU-35 which may have cumulus biotite), implying, that the most evolved nepheline syenites represent fractionated late-stage melts. The fractional crystallization scheme had to be modeled using two stages because the differentiation from the mesocratic nepheline syenite-like parent magma to the least evolved nepheline syenite requires different bulk *D*s' than that required for explaining the variations within the nepheline syenite group. Figure 12 shows the results of the two-stage fractional crystallization model using the REE in combination with Fe. The REE are used to constrain the fractional crystallization scheme because they are relatively immobile and show a strong fractionation within the group which can effectively monitor magmatic crystallization processes. The mineral-melt partition coefficients and their source are listed in Table 5.

Mass balance constraints indicate that the Fe-Mg variations in the first stage of the fractional crystallization process involving differentiation from the mesocratic nepheline syenite-like parent magma to the least evolved nepheline syenite can be explained by fractionating clinopyroxene and amphibole in the weight proportions 37.7 and 55 respectively. The remaining fraction of the assemblage being removed is made up of titanite, apatite, allanite and zircon roughly in the weight proportions 4, 2, 0.7 and 0.7, respectively which can account for the observed depletion in the 'incompatible' trace element concentrations.

The second stage of fractional crystallization which involves differentiation within the nepheline syenites requires lower D values (but still >1) for the REE because of the more gradual decrease in their
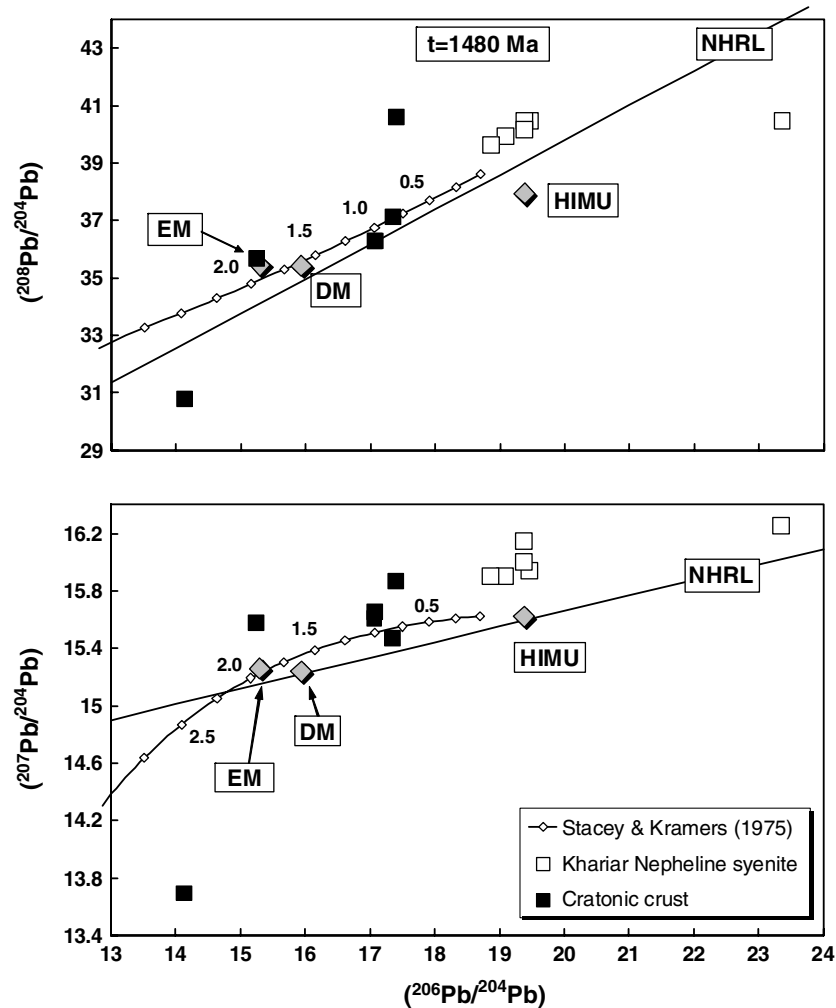
Fig. 11 Pb isotopic ratios of leached feldspar separates from nepheline syenite samples of Khariar. Also shown in the figures are the two-stage terrestrial Pb evolution curves after Stacey and Kramers (1975), the Northern Hemisphere Reference Line (*NHRL*) and the positions of the different mantle reservoirs (Hart 1988; Rehkämper and Hofmann 1997). The isotopic ratios for the DM has been projected back to 1,480 Ma using μ and ω values of 8 and 30 respectively while the enriched mantle (EM-I) and HIMU have been calculated back using μ and ω values of 9 and 35 respectively. Leached feldspar Pb isotope ratios from the cratonic crust are from Rickers et al. (2001). The feldspars from the Khariar nepheline syenites have high $^{207}Pb/^{204}Pb$ and 'normal' $^{208}Pb/^{204}Pb$ which suggest that the source region for the alkaline magma had evolved with a high U/Pb but normal Th/Pb ratios. The isotopic ratios could not have been derived directly from any of the mantle reservoirs or the Bhandara craton crust. The most likely source for the alkaline melt was an enriched mantle domain which had been metasomatised some time prior to the extraction of the alkaline magma

concentrations. Mass balance calculations suggest that the rate of removal of Fe–Mg is broadly similar to the first stage. However, the coherent decrease of the CaO/Al_2O_3 ratio with differentiation (Fig. 5) implies a higher proportion of clinopyroxene in the fractionating assemblage. The Fe_2O_3 and REE variations in this stage can be explained by fractionating an assemblage consisting of about 61.3% clinopyroxene, 35.9% amphibole, 1.3% titanite, 1.1% zircon, 0.3% apatite and 0.1% allanite. The second stage thus involves greater proportions of clinopyroxene and zircon fractionation in comparison to amphibole, titanite, allanite and apatite dominated first stage. Biotite and plagioclase separation was insignificant throughout the evolutionary history and hence do not affect the Fe, Mg contents or the REE.

Petrogenetic model

The formation of an evolved intermediate alkaline magma similar in composition to the mesocratic nepheline syenite-like parent magma at Khariar from an enriched mantle source can be explained by two contrasting models: (1) crystal fractionation of basanite/nephelinite parent magma or (2) fractional crystallization of an alkali basalt magma (Bowen 1928; Baker 1987).
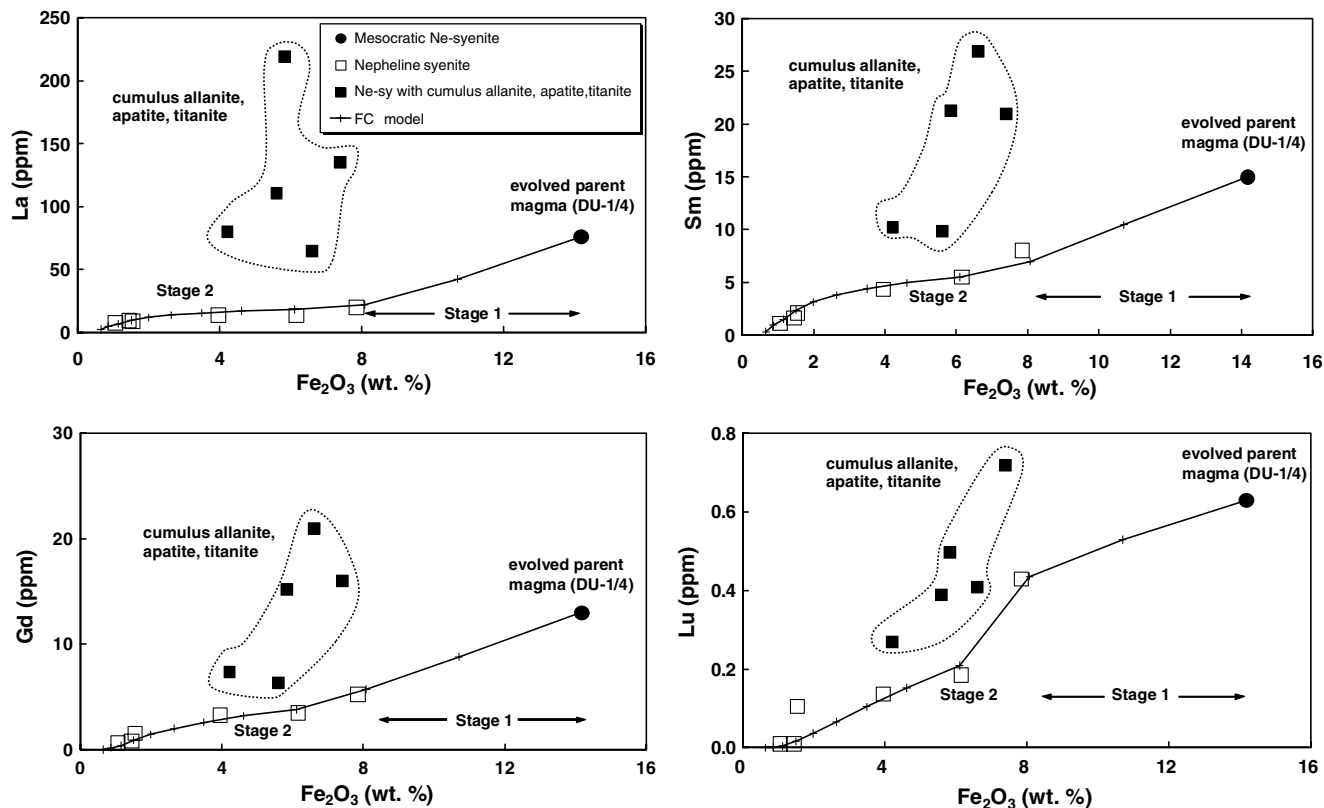
Fig. 12 Results of the fractional crystallization modeling using Fe_2O_3 and the REE on the cumulus phase-free nepheline syenites. The trends can be explained by a two-stage process. The first stage is dominated by the fractionation of amphibole, some clinopyroxene, minor zircon and relatively large amounts of allanite, titanite and apatite. The second stage fractionation is dominated by clinopyroxene, some amphibole, greater amounts of zircon and lesser proportions of allanite, titanite and apatite

Table 5 Mineral-melt distribution coefficients used for modelling the fractional crystallization process

Phase	Fraction	Partition coefficients					References
		La	Sm	Gd	Lu	Fe_2O_3	
Stage 1							
Apatite	0.017	8.6	4.5	15.8	1.7		Paster et al. (1974), Watson and Green (1981)
Titanite	0.040	2.76	59	53.4	3.56		Prowatke and Klemm (2005)
Clinopyroxene	0.377	0.43	0.74	0.89	0.68	22.9	Green and Pearson (1983), Larsen (1979), Nagasawa (1970), Shimizu (1980)
Amphibole	0.552	0.44	0.37	1.72	1.31	28.8	Adam and Green (1994), Matsui et al. (1977)
Zircon	0.007	3.11	4.72	6.4	196		Fujimaki (1986)
Allanite	0.007	820	205	130	7.7		Henderson (1982)
D_{bulk}		6.59	4.43	4.67	2.66		
Stage 2							
Apatite	0.003	8.6	4.5	15.8	1.7		Paster et al. (1974), Watson and Green (1981)
Titanite	0.013	2.76	59	53.4	3.56		Prowatke and Klemm (2005)
Clinopyroxene	0.613	0.43	0.74	0.89	0.68	22.9	Green and Pearson (1983), Larsen (1979), Nagasawa (1970), Shimizu (1980)
Amphibole	0.359	0.44	0.37	1.72	1.31	28.8	Adam and Green (1994), Matsui et al. (1977)
Zircon	0.011	3.1	4.72	6.4	196		Fujimaki (1986)
Allanite	0.001	820	205	130	7.7		Henderson (1982)
D_{bulk}		1.51	1.66	2.13	3.06		

Magmas having the composition of the mesocratic nepheline syenite can form by the fractionation of anorthoclase from a mantle-derived alkaline basaltic primary magma. Such a model has been proposed for the generation of the Ilimaussaq agpaite of the Gardar Alkaline Province in Greenland (Upton 1987; Upton and Emeleus 1987; Paslick et al. 1993). The scheme involving large amounts of plagioclase fractionation

produces characteristic negative Eu anomalies in the rocks which increase with differentiation. However, the Khariar nepheline syenites in general and the mesocratic nepheline syenite in particular do not have prominent negative Eu anomalies which indicate that they did not form by the fractionation of plagioclase from a basaltic parent magma.

Bailey (1987) has suggested that intermediate to salic magmas can form in the sub-continental mantle; a conception which is supported by the occurrence of lherzolite xenoliths in phonolites (Green et al. 1974; Irving and Price 1981) and the presence of phonolitic and trachytic melt in mantle xenoliths (Edgar et al. 1989). Similarly, Green et al. (1974) argue that the 'mafic phonolite lava' (nepheline benmoreite) of Mt. Mitchell rock in Australia having Mg# of about 55 and containing lherzolite inclusions with typical high pressure mineralogy may have formed by crystal fractionation of kaersutitic amphibole as the dominant phase from a basanitic parent magma at high pressure within the upper mantle. The suggestion is supported by Irving (1971) and Irving and Green (1972), who have demonstrated from experimental studies that Ti-rich amphibole together with olivine, clinopyroxene and biotite, occur as near liquidus phases in equilibrium with a basanitic liquid at pressures from 5 to 25 kb. Such a model for the formation of evolved alkaline compositions does not require plagioclase fractionation and can elegantly account for the mantle origin of many felsic to intermediate alkaline liquids. It can also explain the general lack of mafic rocks in many alkaline provinces. Eby et al. (1998) have also suggested a similar high pressure plagioclase-absent fractionation scheme for the formation of the Kasunga-Chipala nepheline syenites and mafic dykes in the North Nyasa Alkaline Province of Malawi. The scarcity of mafic rocks at Khariar together with the geochemical evidence suggesting a mantle origin for the parent magma can be explained by a similar high pressure fractional crystallization scheme outside the plagioclase stability field. Combined fractionation of kaersutitic amphibole and clinopyroxene at mantle pressures from a basanitic primary magma can produce melts lacking a Eu anomaly and with Mg# similar to that of the Khariar mesocratic nepheline syenite.

The basanitic melt parental to the Khariar alkaline rocks may have been produced by the partial melting of a metasomatised sub-continental lithospheric mantle due to the upwelling of the asthenosphere during the initiation of rifting. Significant in-mantle fractionation of the parent alkaline magma continued till the melt density became sufficiently low for the nepheline syenite parent magma to be emplaced in the upper crust. The lack of a negative Eu anomaly and the absence of HREE depletion indicate that the melts were not produced in the plagioclase or garnet stability fields. Hence, it is likely that the source region for the alkaline magma was a part of the spinel lherzolite mantle. As the major part of the magmatic evolution took place at great depths, the observed scarcity of mafic rocks can be accounted for.

Crustal architecture and regional tectonics

Madhavan and Khurram (1989) argue that the alkaline rocks were emplaced at the junction between the cratonic granites to the west and the granulites to the east. The implications are twofold, i.e. the cratonic granites were juxtaposed against the Eastern Ghats Belt during or prior to 1,500 Ma, and therefore, the alkaline rocks and the cratonic granites must have shared the regional Grenvillian granulite-facies metamorphism of the EGP. Both implications are untenable because (a) the exposed regions of alkaline complex record an amphibolite-facies metamorphic overprint, with no evidence of any preceding higher grade assemblage and fabric; the fabric development and metamorphic grade in the granites decrease as traced into the foreland (cf. Gupta et al. 2000; Bhadra et al. 2003, 2004) (Fig. 2) and (b) field evidence such as 'xenolithic' bands of granite within the alkaline rocks suggests that the alkaline magma intruded the granitic basement.

Biswal and Jena (1999) and Biswal et al. (2001) interpreted the boundary between the cratonic rocks and the granulites to represent a collisional thrust in which granulites of the EGP were emplaced as nappes over the cratonic basement. The thrust, marked by an amphibolite-facies ductile shear zone exhibits a wide range of mylonitic fabric with top to the northwest vergent shear movement. Minerals such as amphibole, nepheline and titanite in the shear-related fabric in the nepheline syenites give Pan-African ages. Similarly, monazites occurring in the thrust-induced shear fabric that truncates all earlier structures in the marginal granulites also yield Pan-African ages.

It thus appears that the cratonic domain and the EGP were characterized by independent pre-amalgamation evolutionary histories with the shear related fabric in the marginal zones of the two domains and the alkaline complex recording the effects imposed during Pan-African thrusting of the EGP over the craton. This would mean that the alkaline rocks did not intrude the junction between the EGB and the granites simply because the junction did not exist at 1,480 Ma. Biswal et al. (2001), however, argue that the nepheline syenites were emplaced syn-kinematically during thrusting. It is possible that low-strain domains in the alkaline rocks preserve remnants of an igneous texture, but field and petrographic evidences suggest that the foliation in most parts of the complex is of metamorphic origin and overprints igneous layering. Thus, the idea of syn-kinematic emplacement during thrusting is untenable because the alkaline rocks were emplaced at ~1,480 Ma, while the postulated thrusting of the EGP over the craton is Pan-African in age.

The occurrence of the Khariar and other rift-related alkaline bodies (Upadhyay et al. 2006; Upadhyay and Raith 2006; present study; authors' unpublished data) along the craton-EGB suture poses interesting questions regarding the paleo-tectonic evolution of the contact. Relating the alkaline magmatism to a common geodynamic framework would be crucially dependent on

a temporal relationship between the bodies both in terms of their emplacement and subsequent deformation. The whole-rock radiometric age data (mostly Rb–Sr) of the alkaline rocks reported in earlier studies, however, span a large range from $1,446 \pm 58$ to 856 ± 18 Ma (summarized in Sarkar and Paul 1998) and preclude any temporal correlation. But zircons from four of the alkaline complexes (i.e. Khariar, Kunavaram, Elchuru and Jojuru) spanning the entire length of the suture, dated with SHRIMP and TIMS techniques furnish a much narrower range of concordant to near concordant intrusion ages between 1,480 and 1,262 Ma (Upadhyay et al. 2006; Upadhyay and Raith 2006; present study; authors' unpublished data) which constrains the magmatism to the Mesoproterozoic. The deformation and metamorphism of the complexes were also contemporaneous and took place during the Pan-African tectono-thermal event (Upadhyay et al. 2006; Aftalion et al. 2000; Nagpal et al. 1974; Clark and Subba Rao 1971; Sarkar 1968; present study; authors' unpublished data).

Burke et al. (2003), using a recent compilation of African alkaline igneous rocks and carbonatites, have shown that most of the deformed nepheline syenites and carbonatites (DARCs) are concentrated within known or inferred Proterozoic suture zones. These authors suggest that the well established intracontinental rift setting for the rocks and the likely continental collisional setting for their subsequent deformation, may represent the characteristic features of two well-defined parts of the Wilson cycle. This would mean that the DARCs mark the places where vanished oceans first opened and then closed. The rift related geochemical signatures of the alkaline rocks at the craton-EGB contact zone together with the more constrained geochronological database strongly support a geodynamic scenario involving Mesoproterozoic rifting and Pan-African continental collision in SE India and is remarkably similar to the geodynamic evolution of the DARCs in Africa. The possibility that these alkaline intrusives are the manifestation of a part of a Wilson cycle raises interesting prospects for the formation of an ocean and cratogenic basins where the sedimentary sequences of the EGP and the craton margin basins in peninsular India could have been deposited.

Conclusions

The intrusion of alkaline magma at 1,480 Ma at Khariar marks the initiation of a Mesoproterozoic NE-SW rift along the cratonic margin. The opening of the rift led to the formation of several fault bounded marginal basins and an ocean towards the south. The sediments of the EGP and the craton margin basins (e.g. Chattisgarh basin, Indravati basin) may have been deposited in these rift-related basins. In this context, glauconite from sandstones of the lower Pakhal Group in the NW-SE trending Godavari–Pranhita graben (Fig. 1) gives a K–Ar age of $1,330 \pm 53$ Ma (Vinogradov et al. 1964) which indicates that the Pranhita–Godavari graben may have

formed broadly contemporaneous with the NE-SW Mesoproterozoic rift at the cratonic margin (of which the Khariar alkaline complex represents a part). If the two are related events, the Godavari rift may represent the NW-SE failed arm of a rift system in which the NE-SW trending arm was the active segment.

The Grenvillian orogeny in the EGP is associated with granulite facies metamorphism and tectonism. The accompanying crustal shortening may have been brought about by an inversion of the rift basin. The present crustal geometry at Khariar, however, was achieved only during the Neoproterozoic by the thrusting of the EGP over the cratonic foreland during the Pan-African tectonothermal event. As a consequence, the granites and the alkaline rocks lie in the cratonic footwall with the granulites being juxtaposed against it as a thrust sheet. The lack of a Grenvillian overprint on the cratonic rocks suggests that the amalgamation of the EGP with the Bhandara craton post-dates the Grenvillian tectonothermal event and occurred only during the Pan-African orogeny. However, the possibility of a Grenvillian amalgamation of the two crustal domains cannot be ruled out because the eastern extension of the western fringe region of the rift margin in the cratonic footwall lies below the EGP thrust sheet. Thus, the cratonic margin which would have borne the imprint of the Grenvillian closure may be lying unexposed under the EGP thrust sheet. The broad coincidence in the timing of rifting with subsequent alkaline magmatism at Khariar and the formation of the adjacent Chattisgarh basin may thus not be fortuitous. They may be the result of the same tectonic event where rifting created a passive continental margin on which the Chattisgarh sediments were deposited.

References

Adam J, Green TH (1994) The effects of pressure and temperature on the partitioning of Ti, Sr and REE between amphibole, clinopyroxene and basanitic melts. Chem Geol 117:219–233

Aftalion M, Bowes DR, Dash B, Fallick AE (2000) Late Pan-African thermal history in the Eastern Ghats Terrane, India, from U-Pb and K-Ar isotopic study of the mid-Proterozoic Khariar alkali syenite, Orissa. Geol Surv India Spec Publ 57:26–33

Bailey DK (1987) Mantle metasomatism-perspective and prospect. In: Fitton JG, Upton BGJ (eds) Alkaline igneous rocks. Geological Society Special Publication 30:1–13

Baker BH (1987) Outline of the petrology of the Kenya rift alkaline province. In: Fitton JG, Upton BGJ (eds) Alkaline igneous rocks. Geological Society Special Publication 30:293–311

Bhadra S, Banerjee M, Bhattacharya A (2003) Tectonic restoration of a polychronous mobile belt-craton assembly: constraints from corridor study across the western margin of the Eastern Ghats Belt, India. Memoirs Geol Soc India (Milestone in Petrology) 52:109–130

Bhadra S, Gupta S, Banerjee M (2004) Structural evolution across the Eastern Ghats Mobile Belt-Bastar craton boundary, India. Hot over cold thrusting in an ancient collision zone. J Struct Geol 26:233–245

Biswal TK, Biswal B, Mitra S, Moulik MR (2001) Deformation pattern of the NW terrane boundary of the Eastern Ghats Mobile Belt, India: a tectonic model and correlation with Antarctica. Gondwana Res 5:45–52

Biswal TK, Jena SK (1999) Large lateral ramp in the fold-thrust belts of Mesoproterozoic Eastern Ghats Mobile Belt, Eastern India. Gondwana Res 2:657–660

Bowen NL (1928) The evolution of the Igneous Rocks. Princeton Univ Press, Princeton, pp 334

Burke K, Ashwal LD, Webb SJ (2003) New way to map old sutures using deformed alkaline rocks and carbonatites. Geology 31:391–394

Clark GS, Subba Rao KV (1971) Rb-Sr isotopic age of the Kunavaram Series, a group of alkaline rocks from India. Can J Earth Sci 8:1597–1602

Compston W, Williams IS, Meyer C (1984) U-Pb geochronology of zircons from lunar breccia 73217 using a sensitive high mass-resolution ion microprobe. In: Proceedings 14th lunar planetary science conference. J Geophys Res Suppl 89:B525–B534

Dasgupta S, Sengupta P (2003) Indo-Antarctic correlation: a perspective from the Eastern Ghats Belt. In: Yoshida M, Windley BF, Dasgupta S (eds) Proterozoic East Gondwana: supercontinent assembly and breakup. Geological Society Special Publication 206:131–143

DePaolo DJ (1981) Trace element and isotopic effects of combined wallrock assimilation and fractional crystallization. Earth Planet Sci Lett 53:189–202

DePaolo DJ (1988) Neodymium isotope geochemistry: an introduction. Springer, Berlin Heidelberg New York

Dobmeier JC, Raith MM (2003) Crustal architecture and evolution of the Eastern Ghats Belt and adjacent regions of India. In: Yoshida M, Windley BF, Dasgupta S (eds) Proterozoic East Gondwana: supercontinent assembly and breakup. Geological Society Special Publication 206:145–168

Eby NG, Woolley AR, Din V, Platt G (1998) Geochemistry and petrogenesis of Nepheline Syenites: Kasunga-Chipala, Ilomba and Ulindi nepheline syenite intrusions, North Nyasa Alkaline Province, Malawi. J Petrol 39:1405–1424

Edgar AD, Lloyd FE, Forsyth DM, Barnett RL (1989) Origin of glass in upper mantle xenoliths from the Quaternary volcanics of Gees, West Eifel, Germany. Contrib Mineral Petrol 103:277–286

Fujimaki H (1986) Partition-coefficients of Hf, Zr, and REE between Zircon, Apatite, and Liquid. Contrib Mineral Petrol 94:42–45

Goldstein SL, O'Nions RK, Hamilton PJ (1984) A Sm-Nd study of atmospheric dusts and particulates from major river systems. Earth Planet Sci Lett 70:221–236

Govindaraju K (1994) Compilation of working values and sample description for 383 Geostandards. Geostandard Newslett 18:1–158

Green DH, Edgar AD, Beasley P, Kiss E, Ware NG (1974) Upper mantle source for some hawaiites, mugearites and benmoreites. Contrib Mineral Petrol 48:33–43

Green TH, Pearson NJ (1983) Effect of pressure on rare earth element partition coefficients in common magmas. Nature 305:414–416

Grew ES, Manton WI (1986) A new correlation of sapphirine granulites in the Indo-Antarctic metamorphic terrane: late Proterozoic dates from the Eastern Ghats. Precambrian Res 33:123–139

Gupta S, Bhattacharya A, Raith M, Nanda JK (2000) Contrasting pressure–temperature-deformation history across a vestigial craton-mobile belt boundary: the western margin of Eastern Ghats belt at Deobhog, India. J Metamorphic Geol 18:683–697

Hart SR (1988) Heterogeneous mantle domains: signatures, genesis and mixing chronologies. Earth Planet Sci Lett 90:273–296

Henderson P (1982) Inorganic geochemistry. Pergamon, Oxford, 353 pp

Irving AJ (1971) Geochemical and high pressure experimental studies of xenoliths, megacrysts and basalts from south eastern Australia. Unpublished PhD Thesis, Australian National University

Irving AJ, Green DH (1972) Experimental study of phase relationships in a high-pressure mugearitic basalt as a function of water content, In: Abstracts with Programs. Geol Soc Am 4:550–551

Irving AJ, Price RC (1981) Geochemistry and evolution of high pressure phonolitic rocks from Nigeria, Australia, Eastern Germany and New Zealand. Geochim Cosmochim Acta 45:1309–1320

Jarosewich E, Boatner LA (1991) Rare-earth element reference samples for electron microprobe analyses. Geostandards Newslett 15:397–399

Kale VS (1991) Constrains on the evolution of the Purana basins of Peninsular India. J Geol Soc India 38:231–252

Kale VS (1995) Association of the Purana basin and the middle Proterozoic mobile belts in Peninsular India:Implication of targeting uranium deposits. Explor Res At Miner 8:95–110

Larsen LM (1979) Distribution of REE and other trace-elements between phenocrysts and peralkaline undersaturated magmas, exemplified by rocks from the Gardar Igneous Province, south Greenland. Lithos 12:303–315

Lugmair GW, Shimamura T, Lewis RS, Anders E (1983) Samarium-146 in the early solar system; evidence from neodymium in the Allende Meteorite. Science 222:1015–1018

Madhavan V, Khurram Mohammed ZAK (1989) The alkaline gneisses of Khariar, Kalahandi District, Orissa. In: Leelanandam C (ed) Alkaline rocks. Memoirs Geol Soc India 15:265–289

Matsui Y, Onuma N, Nagasawa H, Higuchi H, Banno S (1977) Crystal structure control in trace element partition between crystal and magma. Tectonics 100:315–324

Mezger K, Cosca M (1999) The thermal history of the Eastern Ghats Belt (India), as revealed by U-Pb and 40Ar/39Ar dating of metamorphic and magmatic minerals: implications for the SWEAT correlation. Precambrian Res 94:251–271

Montel J-M, Foret S, Veschambre M, Nicollet C, Provost A (1996) Electron microprobe dating of monazite. Chem Geol 131:37–53

Münker C, Pfänder JA, Weyer S, Büchl A, Kleine T, Mezger K (2003) Evolution of planetary cores and the earth–moon system from Nb/Ta systematics. Science 301:84–87

Nagasawa H (1970) Rare Earth concentrations in zircon and apatite and their host dacite and granites. Earth Planet Sci Lett 9:359–364

Nagpal MK, Nagpaul KK, Bose MK (1974) Fission track ages of some alkaline rocks of India. J Geol Soc India 15:306–313

Paslick CR, Halliday AN, Davies GR, Mezger K, Upton BGJ (1993) Timing of Proterozoic magmatism in the Gardar Province, southern Greenland. Geol Soc Am Bull 105:272–278

Paster TP, Schauwecker DS, Haskin LA (1974) The behavior of some trace elements during solidification of the Skaergaard layered series. Geochim Cosmochim Acta 38:1549–1577

Platt RG (1996) Nepheline syenite complexes-an overview. In: Mitchell RH (ed) Undersaturated alkaline rocks: mineralogy, petrogenesis and economic potential. Mineralogical Association of Canada, Short Course 24:63–99

Pouchou JL, Pichoir F (1984) A new model for quantitative X-Ray microanalysis, Part I: application to the analysis of homogeneous samples. La Recherche Aérospatiale 3:167–192

Prowatke S, Klemme S (2005) Effect of melt composition on the partitioning of trace elements between titanite and silicate melts. Geochim Cosmochim Acta 69:695–709

Rehkämper M, Hofmann AW (1997) Recycled ocean crust and sediment in Indian Ocean MORB. Earth Planet Sci Lett 147:93–106

Rickers K, Mezger K, Raith MM (2001) Evolution of the continental crust in the Proterozoic Eastern Ghats Belt, India and new constraints for Rodinia reconstruction: implications from Sm–Nd, Rb–Sr and Pb–Pb isotopes. Precambrian Res 112:183–210

Sarkar A, Paul DK (1998) Geochronology of the Eastern Ghats Precambrian mobile belt-a review, Geol Surv India Spec Publ 44:51–86

Sarkar G, Corfu F, Paul DK, McNaughton NJ, Gupta SN, Bishui PK (1993) Early Archean crust in Bastar Craton, central India-a geochemical and isotopic study. Precambrian Res 62:127–137

Sarkar SN (1968) Precambrian stratigraphy and geochronology of Peninsular India. Dhanbad Publishers, India, pp33

Shimizu H (1980) Experimental study on rare-earth element partitioning in minerals formed at 20 and 30 kb for basaltic systems. Geochem J 14:185–202

Simmat R (2003) Identifizierung hochgradig metamorpher Provinzen des Eastern Ghats Belt in Indien anhand einer EMS-Studie von Monazit-Altersmustern. Unpublished PhD Thesis, University of Bonn

Stacey JS, Kramers JD (1975) Approximation of terrestrial lead isotope evolution by a two stage model. Earth Planet Sci Lett 26:207–221

Taylor SR, McLennan SM (1985) The continental crust: its composition and evolution. Blackwell, Oxford

Upadhyay D, Raith MM, Mezger K, Hammerschmidt K (2006) Mesoproterozoic rift-related alkaline magmatism at Elchuru, Prakasam Alkaline Province, SE India. Lithos (in press)

Upadhyay D, Raith MM (2006) Intrusion age, geochemistry and metamorphic conditions of a quartz-monzonite intrusion at the craton-Eastern Ghats Belt contact near Jojuru, India. Gondwana Res (in press)

Upton BGJ (1987) Gabbroic, syenogabbroic and syenitic cumulates of the Tugtutoq younger Giant Dyke Complex, south Greenland. In: Parsons I (ed) Origins of igneous layering. Reidel, Dordrecht-Boston, NATO ASI Series, Series C. Math Phys Sci 196:93–123

Upton BGJ, Emeleus CH (1987) Mid-Proterozoic alkaline magmatism in southern Greenland; the Gardar Province. In: Fitton JG, Upton BGJ (eds) Alkaline igneous rocks. Geological Society Special Publication 30:449–471

Vinogradov AP, Turgarino AI, Zhjkov C, Stapnikova N, Bibikova E, Khores K (1964) Geochronology of Indian Precambrian. In: 10th Int Geol Congr New Delhi, pp 553–567

Wasserburg GJ, Jacobsen SB, DePaolo DJ, McCulloh MT, Wen J (1981) Precise determinations of Sm/Nd ratios, Sm and Nd isotopic abundances in standard solutions. Geochim Cosmochim Acta 45:2311–2323

Watson EB, Green TH (1981) Apatite/liquid partition coefficients for the rare earth elements and strontium. Earth Planet Sci Lett 56:405–421

Zuleger E, Erzinger J (1988) Determination of the REE and Y in silicate materials with ICP-AES. Fresenius Zeitschrift für Analytische Chemie 332:140–143